Palaeogeography, Palaeoclimatology, Palaeoecology 607 (2022) 111264

Contents lists available at ScienceDirect

Palaeogeography, Palaeoclimatology, Palaeoecology

journal homepage: www.elsevier.com/locate/palaeo

Isotopic time-series ($\delta^{13}C$ and $\delta^{18}O$) obtained from the columnar layer of Permian brachiopod shells are a reliable archive of seasonal variations

Claudio Garbelli [a,b,*], Lucia Angiolini [c], Renato Posenato [d], Elizabeth M. Harper [a], Miles D. Lamare [e], Guang R. Shi [f], Shu-zhong Shen [g,**]

[a] Department of Earth Sciences, University of Cambridge, Cambridge CB2 3EQ, UK
[b] State Key Laboratory of Palaeobiology and Stratigraphy, Nanjing Institute of Geology and Palaeontology and Center for Excellence in Life and Paleoenvironment, Chinese Academy of Sciences, 39 East Beijing Road, Nanjing 210008, China
[c] Dipartimento di Scienze della Terra "A. Desio", Università degli Studi di Milano, Via Luigi Mangiagalli, 34, Milan, Italy
[d] Dipartimento di Fisica e Scienze della Terra, Università di Ferrara, Via Saragat 1, I-44121 Ferrara, Italy
[e] Department of Marine Science, University of Otago, PO Box 56, Dunedin, New Zealand
[f] School of Earth, Atmospheric and Life Sciences, University of Wollongong, Northfields Ave, NSW 2522, Australia
[g] State Key Laboratory for Mineral Deposits Research, School of Earth Sciences and Engineering and Frontiers Science Center for Critical Earth Material Cycling, Nanjing University, Nanjing 210023, China

ARTICLE INFO

Editor: Dr. Howard Falcon-Lang

Keywords:
Sclerogeochemistry
Seawater temperature seasonality
Carbon and oxygen isotope proxies
Biogenic carbonate geochemistry

ABSTRACT

In this paper, we develop a robust palaeo-proxy technique for inferring seasonal fluctuations in Phanerozoic seawater temperature. Specifically, we report $\delta^{13}C$ and $\delta^{18}O$ values across the columnar layer (inner shell) of Permian brachiopods, including five genera of the Order Spiriferida (*Ingellarella*, *Martinia*, *Permophricodothyris*, *Cartorhium*, and *Trigonotreta*) and two genera of the Order Athyridida (*Araxathyris* and *Comelicania*). These brachiopod specimens are inferred to have inhabited varied palaeo-depths, based on facies analysis, and were collected from low, middle and high palaeolatitudes. To obtain high-resolution ontogenetic isotopic time-series, a handheld microdrill was used to collect low-magnesium calcite samples along the longitudinal axis of the mid-valve for each specimen. Intrageneric and intergeneric comparison of statistics (mean values, variance, and range) reveals that $\delta^{18}O$ values are consistent within and between genera although $\delta^{13}C$ values are more variable. In specimens obtained from low palaeolatitudes (Julfa Formation, Iran; Bellerophon Formation, Italy; Late Permian), the range of $\delta^{18}O$ values is small and consistent with weak seasonal temperature variations, irrespective of water depth. In specimens obtained from middle palaeolatitudes (Qarari Formation, Oman; Early-Middle Permian), we found a range of $\delta^{18}O$ values dependent on inferred water depth, possibly reflecting a change in thermocline structure between warm and cold seasons. In specimens obtained from high palaeolatitudes (Wasp Head and Wandrawandian Siltstone formations, Australia; Early-Middle Permian), brachiopods from glacial and interglacial climate phases show significant variations of $\delta^{18}O$ values, probably caused by seasonal changes in the seawater surface temperature. Based on these findings, the technique developed in this paper appears to provide reliable paleoclimate and paleoenvironmental data for Permian sites, and should be also applicable for Phanerozoic studies in general. However, we caution that $\delta^{18}O$ values vary dependent on the growth direction, resulting in differences of up to 5 °C in seawater paleotemperature calculations, and emphasise that a consistent sampling strategy accounting for shell structure and growth direction is required.

1. Introduction

Sclerogeochemistry is a useful technique to understand the seasonality of past climate in marine contexts (Butler and Schöne, 2017). In marine settings, the hard parts of calcifying accretionary organisms, such as bivalves, brachiopods, gastropods, and corals, allow the reconstruction of paleoenvironmental time series at high temporal resolution (Schöne and Surge, 2012). However, obtaining reliable

* Corresponding author at: Department of Earth Sciences, University of Cambridge, Cambridge CB2 3EQ, UK.
** Corresponding author.
E-mail addresses: cg772@cam.ac.uk (C. Garbelli), szshen@nju.edu.cn (S.-z. Shen).

https://doi.org/10.1016/j.palaeo.2022.111264
Received 3 July 2022; Received in revised form 30 September 2022; Accepted 30 September 2022
Available online 6 October 2022

paleoenvironmental archives is more challenging with increasingly ancient materials.

For Paleozoic study intervals, the shells of rhynchonelliformean brachiopods are considered one of the most robust archives for $\delta^{18}O$ values and the reconstruction of seawater temperature fluctuations (Brand et al., 2011; Immenhauser et al., 2016, and references therein). The brachiopod shell has an excellent potential to preserve its original chemical and structural composition because it is of low magnesium calcite (brachiopod low-Mg calcite shells; herein bLMC shells) composition, which is diagenetically most resistant form of $CaCO_3$ (Brand and Veizer, 1980; Al-Aasm and Veizer, 1982; Popp et al., 1986; Brand, 2004; Casella et al., 2018). Brachiopods have various types of shell fabric (e.g. Cusack and Williams, 2001). Rhynchonelliformeans have a two- or three layered shells, the former with a dendritic primary layer followed by a fibrous or laminar secondary layer, whereas the latter with an additional columnar layer (tertiary layer).

The columnar layer is generally the best preserved because (a) it develops in the innermost part of the shell, and (b) it contains a very small quantity of organic matter and, as a result, is highly compact (Mii and Grossmann, 1994; Angiolini et al., 2012; Garbelli et al., 2012, 2014, 2019; Rollion-Bard et al., 2019). The columnar layer is present in numerous extinct and extant taxa, and it has been described in many genera of most orders of the classes Rhynchonellata and Strophomenata, the two most widespread Paleozoic groups (Williams, 1968; Mackinnon, 1974; Angiolini et al., 2012, 2019; Garbelli, 2017). The fabric and microstructure of the columnar layer are very similar across the various taxa, making the columnar layer an analogous structure. Another important feature of bLMC is that multi-proxy tools may be applied to test, qualify, and quantify preservation and alteration (Brand et al., 2011), allowing for screening of diagenesis.

Early studies suggested that brachiopods biomineralize their shell from body fluids that are chemically similar to seawater, without any vital effect (Lowenstam, 1961). However, there is growing evidence that growth rate and biological (metabolic) effects do result in some oxygen isotopic disequilibrium with isotopic equilibrium retained only in specific parts of the bLMC shell (Auclair et al., 2003; Yamamoto et al., 2010, 2013; Cusack et al., 2012; Takayanagi et al., 2012, 2013; Immenhauser et al., 2016; Romanin et al., 2018; Rollion-Bard et al., 2019). In extant species, the innermost secondary layer and the columnar layer have $\delta^{18}O$ values in the range of equilibrium values and may be used as a reliable thermometer of seawater (Cusack et al., 2012; Brand et al., 2019). This shell layer is likely precipitated at slower growth rates, and not affected by kinetics (Rollion-Bard et al., 2019); thus, the fractionation effect due to physiological controls on oxygen isotopic composition should be minimal in this portion of the shell.

Another advantage of targeting bLMC shells is that brachiopods are sessile organisms for most of their life span (apart from a possible short-lived larval phase in some species); therefore, they are static recorders of the surrounding environment. High-resolution profiles of $\delta^{18}O$ values along the growth direction of the shell of the extant taxon *Terebratulina crossei* Davidson, 1882 record an oscillatory signal related to seasonal changes in seawater temperature (Takayanagi et al., 2015). Moreover, the isotopic composition of the columnar layer of specimens of extant *Liothyrella neozelanica*, Thomson 1918, recovered from different water depths, shows depth-related variations of the temperature while trace element analysis allows identification of a seasonal component (Butler et al., 2015). Therefore, extant brachiopods represent a robust archive of short-term environmental variability and seasonality (Powell et al., 2009); however, whether these characteristics can be applied to Paleozoic archives requires further testing.

Only a few studies have explored the extent to which $\delta^{18}O$ values record seasonal variations in Paleozoic brachiopod shells (Mii and Grossmann, 1994; Angiolini et al., 2012; Roark et al., 2016), but none has specifically focused on the columnar layer or developed a consistent sampling strategy. The aim of this paper is therefore to describe and test a sampling strategy to be used consistently in future investigations related to the study of Permian climate and environments, a strategy that can be eventually extended to fossil brachiopods of other periods of time.

Specifically, in this paper, (1) we report the oxygen and carbon isotope composition ($\delta^{18}O$ and $\delta^{13}C$) of the columnar layer of taxa of Permian Athyridida and Spiriferida, using a consistent sampling strategy for different species from low, mid- and high paleolatitudes; (2) we ascertain if the signal recorded in the columnar layer shows common patterns and test the isotope ratio signal at intraspecific and interspecific levels; (3) we critically assess whether the $\delta^{18}O$ values of the columnar layer provide reliable information about seasonal seawater temperature variations for the surrounding environment by analyzing statistical parameters such as mean, variance and range. We also analyze a portion of the columnar layer in a modern Terebratulida, *Liothyrella neozelanica*, Thomson 1918, one of the two extant species known to have a columnar layer, to verify the extent to which selected statistical parameters approximate to the seasonality of the living environment.

2. Material and methods

2.1. Provenance of the material

This study focuses on a detailed analysis of 11 brachiopod specimens from Permian succession across a range of palaeolatitudes (Table 1; Supplementary Fig. S1). Material includes species of five genera of thick-shelled brachiopods of the Order Spiriferida (*Ingellarella*, *Martinia, Permophricodothyris*, *Cartorhium*, *Trigonotreta*), and of two genera belonging to the Order Athyridida (*Araxathyris* and *Comelicania*).

Specimens of *Trigonotetra* sp. (Tri-WH-1, Tri-WH-2, Tri-Ww) were collected from the Wasp Head Formation and Wandrawandian Siltstone, and *Ingelarella* sp. (Ing-Ww) from the Wandrawandian Siltstone in the southern Sydney Basin (Cisterna and Shi, 2014). The Wasp Head Formation is considered Asselian-Sakmarian in age based on macrofossils and Sr isotope ratios ($^{87}Sr/^{86}Sr$) of the brachiopods shells (Garbelli et al., 2019) and a recent reassessment of the chronostratigraphy employing geochronology and biostratigraphy (Shi et al., 2022). The specimens were collected from the top of the South Durras outcrop (horizon WH-B-1 in Garbelli et al., 2019), where the succession consists of pebbly sandstones and siltstones, intercalated with diamictites; upward, siltstones become dominant (Shi et al., 2010). Facies analysis suggests that the upper Wasp Head Formation was deposited below fair weather wave base, and above the storm-wave base, in the offshore-transition zone (Rygel et al., 2008).

The Wandrawandian Siltstone is latest Kungurian to Roadian in age (Shi et al., 2022). The succession is mostly composed of siltstones, locally intercalated with sandstones. At Warden Head near Ulladulla, the sedimentary succession is composed of, from base to top, pebbly sandstones and siltstones; synsedimentary slumps (seismites), sandstone wedges, and diamictite lenses, and siltstones without slumping structures, with rare pebbles and rich in fossils (Shi et al., 2007). The specimens labeled Tri-Ww and Ing-Ww were collected at Dolphin Point and Penguin Head, respectively; in the former locality the lower part of Wandrawandian Siltstone outcrops, while, at Penguin Head, its upper part is exposed. The sediments have been inferred to be deposited at depth comprised between the fair weather wave base and the storm wave base (Thomas et al., 2007). The two localities are slightly different in age, but both fall within the glacial phase P3 of Fielding et al. (2008).

The specimens belonging to *Permophricodothyris* sp. (Per-Ju-1, Per-Ju-2), and *Araxathyris* sp. (Ara-Ju) were collected from the *Permophricodothyris ovata* Zone of the Julfa Formation in northwestern Iran (Ghaderi et al., 2014). This formation is Wuchiapingian in age based on conodonts (Henderson et al., 2008; Shen and Mei, 2010) and ammonoids (Ghanizadeh Tabrizi et al., 2022), and consists of gray to red shales with nodular limestones, which record an overall deepening trend, reaching outer ramp conditions, at depth around the storm wave base (Leda et al., 2014). The specimens belong to a relatively narrow

Table 1
Summary of the fossil specimens analyzed in this study: taxonomy, stratigraphic unit, and time interval.

Specimen	Order	Genera	Stratigraphic horizon	Source	Formation	Specimen Age range	Paleogeographic position and setting
Tri-WH-1	Spiriferida	*Trigonotreta*	WH-B-1	Garbelli et al., 2019	Wasp Head Formation - Sydney Basin, Australia	Late Sakmarian (289.6 ± 1.5)	southern high paleolatitudes (~60°S); Panthalassa Ocean; nearshore/offshore marine; depths between fair weather base and storm wave base
Tri-WH-2	"						
Tri-Ww	"		WW-B-8		Wandrawandian Siltstone - Sydney Basin, Australia	Latest Kungurian - Roadian (265.2 ± 0.6 to 263.1 ± 1.1	
Ing-Ww	"	*Ingelarella*	WW-B-20				
Car-WKJ	"	*Cartorhium*	WKJb-302	Viaretti et al., 2022	Qarari unit - Oman	Late Kungurian (274 to 268.8)	subtropical paleolatitudes (~30); opening branch of the Neotheys ocean; depths around the storm wave base
Mar-WKJ	"	*Martinia*	WKJf-14				
Per-Ju-1	"	*Permophricodothyris*	G 144	Ghaderi et al., 2014	Julfa Formation - Ali Bashi Mountains Northwestern Iran	Early Wuchiapingian (259.8–257)	equatorial paleolatitudes; Neothetys ocean; depths around the storm wave base
Per-Ju-2	"						
Ara-Ju	Athyridida	*Araxathyris*	G 143				
Com-Bel-1	Athyridida	*Comelicania*	VB8B	Brand et al., 2012, Garbelli et al., 2022a	Bellerophon Formation - Dolomites, Northern Italy	Late Changhsingian (251.9)	equatorial paleolatitudes; Neothetys ocean, very restricted basin; near to offshore marine; depths near the base of fair-weather waves
Com-Bel-2	Athyridida		WPK10				

stratigraphic interval of the lower Julfa beds, comprised between the horizons G140 and G154 (see Fig. 4 in Ghaderi et al., 2014), which is ~6 m thick.

Specimens of *Cartorhium* aff. *multiradiatus* Reed, 1944 (Car-WKJ) and *Martinia* sp. (Mar-WKJ) have been collected in the Wadi Khawr al Jaramah outcrop, which belongs to the Qarari Unit (Batain Group) in northeastern Oman. Fusuline biostratigraphy indicates that this stratigraphic unit is Kubergandian in age (Leven and Heward, 2013). Based on the correlation of the Tethyan stages with the ISC timescale (Angiolini et al., 2015), the unit is Kungurian-Roadian in age. Recent data, based on brachiopod assemblages from Wadi Khawr al Jaramah, suggest that the Qarari Unit straddles the Cisuralian-Guadalupian boundary (Viaretti et al., 2022). The Wadi Khawr al Jaramah outcrop consists of a weathered surface of a 450 m^2 of yellowish and highly fossiliferous marly limestones (Fortey and Heward, 2015). The Qarari Unit has been interpreted to have been deposited at depths around the storm wave base (Leven and Heward, 2013; Viaretti et al., 2022).

The specimens of *Comelicania* sp. (Com-Bel-1, Com-Bel-2) were collected in the upper *Comelicania* beds located in the Bulla Member of the Bellerophon Formation in northern Italy (Posenato, 2001, 2010). The two specimens belong to different successions located in Val Brutta and Sass the Putia, northern Italy. The Bulla Member represents the time interval just before the end-Permian mass extinction (Brand et al., 2012; Posenato, 2019; Garbelli et al., 2022a). The Bulla member consists of blackish bioclastic wackestones, packstones, and marlstones with abundant fossils recording a very shallow marine environment, few metres deep, located near the base of fair weather waves (Farabegoli et al., 2007; Posenato, 2009, 2019). The conodonts suggest a latest Changhsingian age (Farabegoli and Perri, 1998) as well age estimation using $^{87}Sr/^{86}Sr$ ratio measured on fossil brachiopods (Garbelli et al., 2022a).

The modern *Liothyrella neozelanica* (Lio-DS) was collected by SCUBA at Tricky Cove in Doubtful Sound, New Zealand (45.3456 S, 167.0423 E) at water depth equal to ~17 m on 9 December 2020.

2.2. Specimens selection and preparation

The specimens analyzed for this study represent different taxa, time intervals, and paleolatitudes (Fig. 1, Table 1). These specimens were selected based on previous knowledge about their shell microstructure and preservation (Garbelli et al., 2012, 2019; Brand et al., 2012; Mii et al., 2012; Angiolini et al., 2008; Stephenson et al., 2012). Cisuralian and Guadalupian Permian brachiopods from the southern Sydney Basin (Australia), as well as Lopingian brachiopods from Iran and the Dolomites, have already been shown to display excellent preservation of the shell (Garbelli et al., 2012, 2019; Brand et al., 2012; Mii et al., 2012).

Ongoing microstructural analyses of Wadi Khawr al Jaramah brachiopods of Oman by one of the authors (LA) show that the columnar layer is well preserved, except for local silicification which does not cause alteration of the carbonate, only replacement, in fact shielding the enclosed calcite from later diagenesis. This is in line with the observation that fossil brachiopods from other Cisuralian and Guadalupian localities of Oman usually retain a very good preservation of the shell microstructure, and their geochemical composition is considered representative of the living environment (Angiolini et al., 2008; Stephenson et al., 2012).

For all specimens, the ventral valve was chosen as the sampling target since it is usually thicker than the dorsal valve (e.g., Angiolini et al., 2019), and it is thus easier to sample. All the selected taxa developed a relatively large shell, with a columnar layer, underlying a fibrous one (Cusack and Williams, 2001).

The selected specimens were embedded in epoxy resin and sectioned along the mid-shell longitudinal axis, perpendicular to the outer shell surface, using a diamond blade cutter. One slab was selected as the target for collecting the samples for geochemical analyses; this slab was polished under 0.3 μm alumina etched with 5% of HCL for 5 s, rinsed with flushing water, dried, and then coated to be inspected with the LEO 1530 VP scanning electron microscope (SEM). This slab was subsequently re-polished to observe structural features, such as evident growth lines, micro-fractures, or other shell defects under a binocular microscope during the collection of samples. The opposite slab was mounted and cut as a thin section, and then polished using successively finer grits down to 0.3 μm de-agglomerated alpha-alumina and inspected with a Nuclide ELM2 cathodoluminescence microscope system (CL) operating at 10 kV with a beam current of 5–7 mA. Exposure to the electronic beam (before taking the photo) was on the order of 15–30 s.

2.3. Shell sampling and geochemical analyses

A shell section was drilled using a hand-held micro drill equipped with a carbide bit. The drillings have been performed on the polished slab in the topmost part of the columnar layer, just below the fibrous layer (Fig. 2), and arranged parallel to the posterior-anterior growth direction to obtain longitudinal transects representing ontogenetic time-series (Figs. 2, S1, S2). The sampling strategy follows the one employed on recent brachiopod specimens by Yamamoto et al. (2013) and

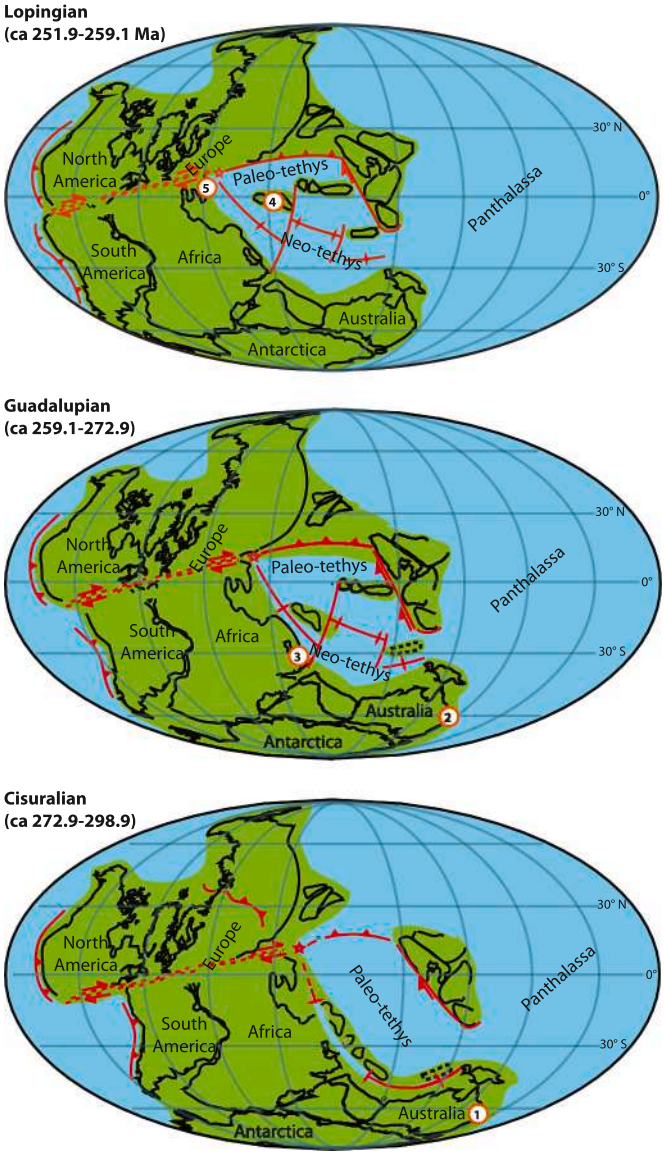

Fig. 1. Paleogeographic reconstructions showing the location of the stratigraphic units where the investigated brachiopod specimens were collected. Modified after Muttoni et al., 2009, Angiolini et al., 2015.

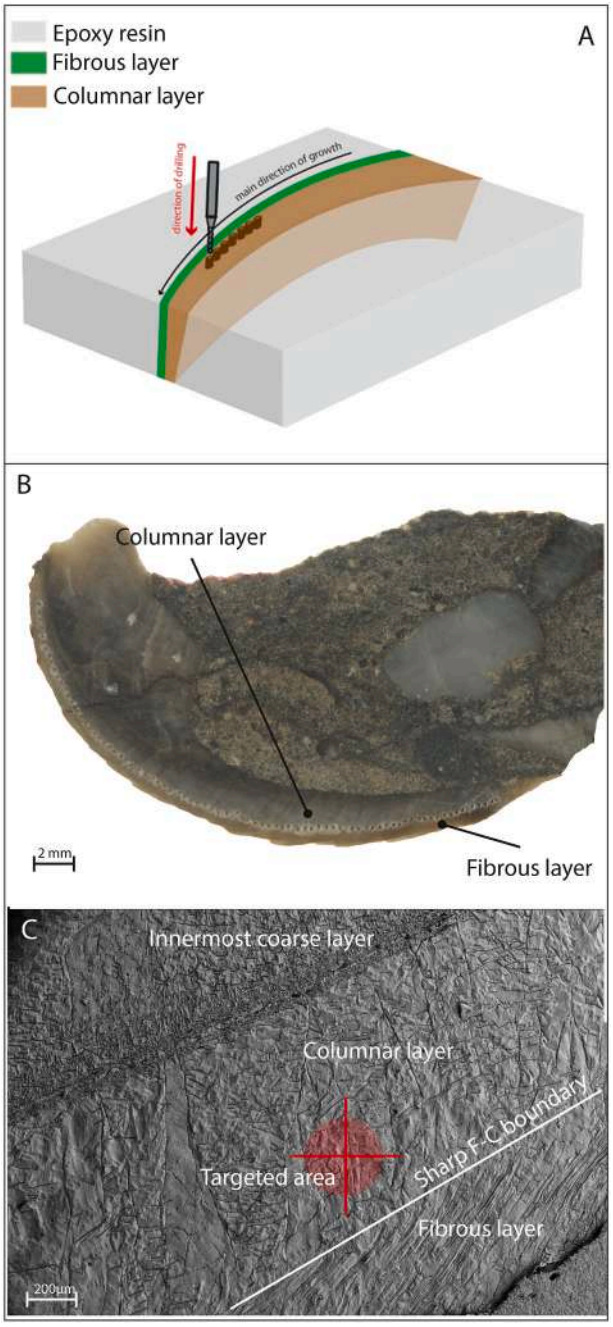

Fig. 2. A) Schematic illustration showing the strategy of sampling; B) section of a ventral valve embedded in epoxy resin and polished, showing the sequential drilled samples along the longitudinal axis, specimens Tri-WH-2; C) detail of the anterior shell margin of Tri-WH-2 at the SEM before drilling, showing the main features of the targeted area, from which the shell material was sampled using the hand drill bit.

Takayanagi et al. (2015) (Fig. 2A; see Supplement fig. EA1 in Takayanagi et al., 2015). The drillings were performed in the columnar layer just below the fibrous layer (Fig. 2C), to sample the same phase of the shell microstructure, i.e., after the change in the secretory regime governing the transition from the fibrous to the columnar layer. The drillings were performed under a binocular microscope, mapping the position of sample along the shell section. Additional information was recorded if the drill hole was in a portion suspected of alteration caused by the proximity to micro-fractures or regions permeated by diagenetic fluids, alongside scrutiny from the CL analysis of the opposite slab. The specimens were rinsed with ultrapure water and dried after each drilling to avoid cross-contamination between nearby samples. Finally, based on a comparison of the information from SEM, CL analyses on the opposite slab and the optical evaluation, each sample was assessed as potentially preserving the original geochemical signal or altered.

For the analysis of $\delta^{13}C$ and $\delta^{18}O$ values, ~100 µg of calcite powder were obtained using a drill bit of 0.2 mm in diameter, resulting in a sample hole of ~250 µm in diameter, which extends about 700–800 µm in depth. To further evaluate the potential effect of diagenesis, a subset of samples was analyzed for trace and minor elemental composition (Mg, Sr, Fe, Mn). This subset comprised samples judged potentially bearing the original signal after optical screening under the binocular microscope, CL and SEM, as well as those deemed altered. A drill bit of 0.3 mm was used to gain a large quantity of powder (~200 µg), which is necessary to measure both trace elements and isotopes and to avoid sampling too deeply.

About 100 µg of powder was reacted with ultrapure 100% HPO_3 at 72.2 °C to release CO_2 in a Kiel IV automated carbonate reaction device, coupled with a Finnigan MAT 253 mass spectrometer to measure $\delta^{13}C$ and $\delta^{18}O$ values. Long-term precision and accuracy compared to NBS19

standard values ($n = 668$, $\delta^{13}C = +1.95‰$, $\delta^{18}O = -2.20‰$) were better than 0.03‰ (2sd) for $\delta^{13}C$ and 0.08‰ (2sd) for $\delta^{18}O$.

Minor and Trace element content (Mg, Sr, Mn, Fe) was determined using a Quadrupole ICP-MS (Agilent 7700×) instrument. A multipoint calibration using a blank and seven calibration solutions, covering the expected range of the concentration of the sample, was employed. The accuracy was verified by multiple analyses of the international reference materials JLs-1 and JDo-1 (Imai et al., 1996). Samples and standard powders were weighted with a Mettler Toledo XP6 microbalance (readability = 0.001 mg, repeatability = 0.0004 mg, minimum weight = 0.08 mg). Aliquots of ~100 μg were dissolved in 1 ml of 0.2 M HNO_3 and reacted for 70 min. Subsequently, the internal standard was added. The long-term reproducibility RSD (relative standard deviation 2σ) is better than 4% for Mg, Sr, Mn, and 6% for Fe, assessed by repeated measurements of carbonate reference materials JDo-1 (Mg = 18.47%, Sr = 0.0116%, Mn = 0.00657%, Fe = 0.0222%) and JLs-1 (Mg = 0.606%, Sr = 0.0295%, Mn = 0.00209%, Fe = 0.0178%). The analyses have been performed at the Nanjing Institute of Geology and Palaeontology of the Chinese Academy of Sciences between 2018 and 2019.

The analysis of the modern *Liothyrella neozelanica* has been subsequently performed at The Godwin Laboratory for Palaeoclimate Research, Department of Earth Sciences, University of Cambridge Analyses. Approximately 50–200 micrograms of dried homogenised sample was transferred in to Exetainer vials and sealed with silicone rubber septa using a screw cap. The samples were flushed with CP grade helium then acidified with 104% orthophosphoric acid, left to react for 1 h at 70° Celsius and then analyzed using a Thermo Gasbench preparation system attached to a Thermo Delta V Advantage mass spectrometer in continuous flow mode. Each run of samples was accompanied by 10 reference carbonates (Carrara Z) and 2 control samples (Fletton Clay). Carrara Z has been calibrated to VPDB using the international standard NBS19. The results are reported with reference to the international standard VPDB and the precision is better than +/− 0.08 per mil for $\delta^{13}C$ and +/− 0.10 per mil for $\delta^{18}O$.

2.4. Statistical analyses

To quantify the reliability of the evaluation based on SEM, CL and optical screening, we performed a cluster analysis based on Mg, Sr, Fe and Mn content, obtaining two groups classified as 'preserved' or 'altered, based on the comparison with previously published data from the same localities (Brand et al., 2012; Garbelli et al., 2012, 2014, 2016, 2019, 2022a), and also taking into account the concentration range observed in modern brachiopods (Brand et al., 2003). Then, we calculated the percentage of misplaced samples, i.e. those judged as potentially 'preserved' combining SEM, CL and optical screening, but included in the 'altered' cluster based on elemental values and, conversely, the spurious incorporated in the cluster of 'preserved'. Details of the employed method are provided in the Supplementary Materials.

We evaluated the correlations of $\delta^{13}C$ and $\delta^{18}O$ values employing the reduced major axis regression technique (Sokal and Rohlf, 1994). The significance of the correlation was examined using the two-sided Pearson test, with a 99% confidence limit. Since the mean growth rate of rhynchonelliformean brachiopods slows down with aging (Takayanagi et al., 2015; Garbelli et al., 2022b), we calculated a linear regression model to evaluate the effect of the position along the shell length transect on the oxygen isotopic composition and to estimate the presence of significant effect related to the growth for those samples deemed preserved. An alternative linear model was calculated after decomposing the signal into Intrinsic Mode Functions (IMFs), using the Hilbert Huang Transform (Huang et al., 1998). This analysis provides information about the frequencies of oscillation and quantifies the amount of variation at different time scales. The residue is the lower frequency signal embedded in the time series (the trend or the baseline signal), thus it should embed the long-term change in the rate of accretion due to aging. In fact, at the timescale of brachiopods life cycle (a few to several tens of years, e.g. Angiolini et al., 2012; Baird et al., 2013), the environmental signals show shorter natural cycles (daily to yearly) than those related to change in the growth from juvenile to adult up to the gerontic stage. The mean and variance, range of overlaps between specimens belonging to the same sedimentary succession, skewness, and variance of the residuals and of the de-trended time series were calculated to evaluate the differences in the seasonal signal of the $\delta^{18}O$ values between specimens and localities.

To calculate the mean seasonal difference in seawater surface temperature (ΔSST) from $\delta^{18}O$ values we employed two different equations. The first one is from Watkins et al. (2014) and it is calibrated on inorganically precipitated calcite:

$$\Delta^{18}O^{eq}_{c-sw} = \frac{17747}{T_k} - 29.777 \quad (1)$$

This first equation works well when employed with the $\delta^{18}O$ values of the columnar layer of brachiopods (Rollion-Bard et al., 2019). The second one is the equation proposed by Brand et al. (2019):

$$T^{\circ}C = 17.375 - 4.2535\left(\Delta^{18}O_c - \Delta^{18}O_{sw}\right) + 0.1473\left(\Delta^{18}O_c - \Delta^{18}O_{sw}\right)^2 \quad (2)$$

This second equation is calibrated using modern brachiopods shells of different species living in a wide range of temperature and employing mostly the fibrous layer, because the columnar has been only reported in two living species up to date.

3. Results

3.1. Evaluation of preservation

3.1.1. Shell microstructure and cathodoluminescence

The analyzed ventral valves comprise a fibrous layer with an underlying columnar layer. The outer fibrous layer consists of fibers with keel and saddle outlines and regular spaces between each unit (Figs. 3A-B-C-D-E). The shells of the spiriferides (*Martinia* and *Cartorhium*) from Oman show localized silicification of the outermost fibers, with silica deposited in the spaces between the fibers, where organic tissues were originally present (Fig. 3E, S3). The transition from fibers to columns is sharp in the spiriferids (*Ingellarella*, *Martinia, Permophricodothyris*, *Cartorhium*, and *Trigonotreta*; Fig. 3G-H-I), and in the athyridid *Comelicania*, but it is more gradual in species of *Araxathyris*. The columnar layer is developed up to two-thirds of the length in species of *Ingellarella* and *Trigonotreta.* In species of *Cartorhium*, *Permophricodothyris* and *Martinia*, the columnar layer of the anterior part becomes progressively thinner. The columnar layer is localized only in the posterior region in species of *Araxathyris*. The thickness of the columnar layer is different in the analyzed specimens. The specimens from the Sydney Basin have the thickest columnar layer, (> 2 mm in species of *Trigonotreta* and *Ingelarella*). At half to two/thirds of the shell length of species of *Trigonotreta* and *Ingellarella*, the fibers gradually replace the columns (Fig. 3L), forming a wider angle with the outermost surface (compare Fig. 3M with Fig. 3N), and larger units through the amalgamation of adjacent elements (Fig. 3O).

Spiriferid and athyridid specimens have well-preserved columns, with growth bands frequently observable in all investigated specimens (Fig. 3P). Locally, the columns display coarse surfaces, which indicate a localized alteration of the microstructure (Fig. 3Q). The region of the shell thickness with consistently good micro-morphological preservation is the one just underlying the fibrous layer, or the middle part of the thickness of the columnar layer. The innermost part, which is adjacent to the sediment or cement filling, is often poorly preserved (Fig. 3R). In the specimens from the Sydney Basin, the innermost part of the shell shows a coarse texture, as well as in the region of contact between the dental plate and the columnar layer in the posterior part of the shell, where a discontinuity is always present (Fig. 3S).

The CL analysis of the studied spiriferid and athyridid specimens

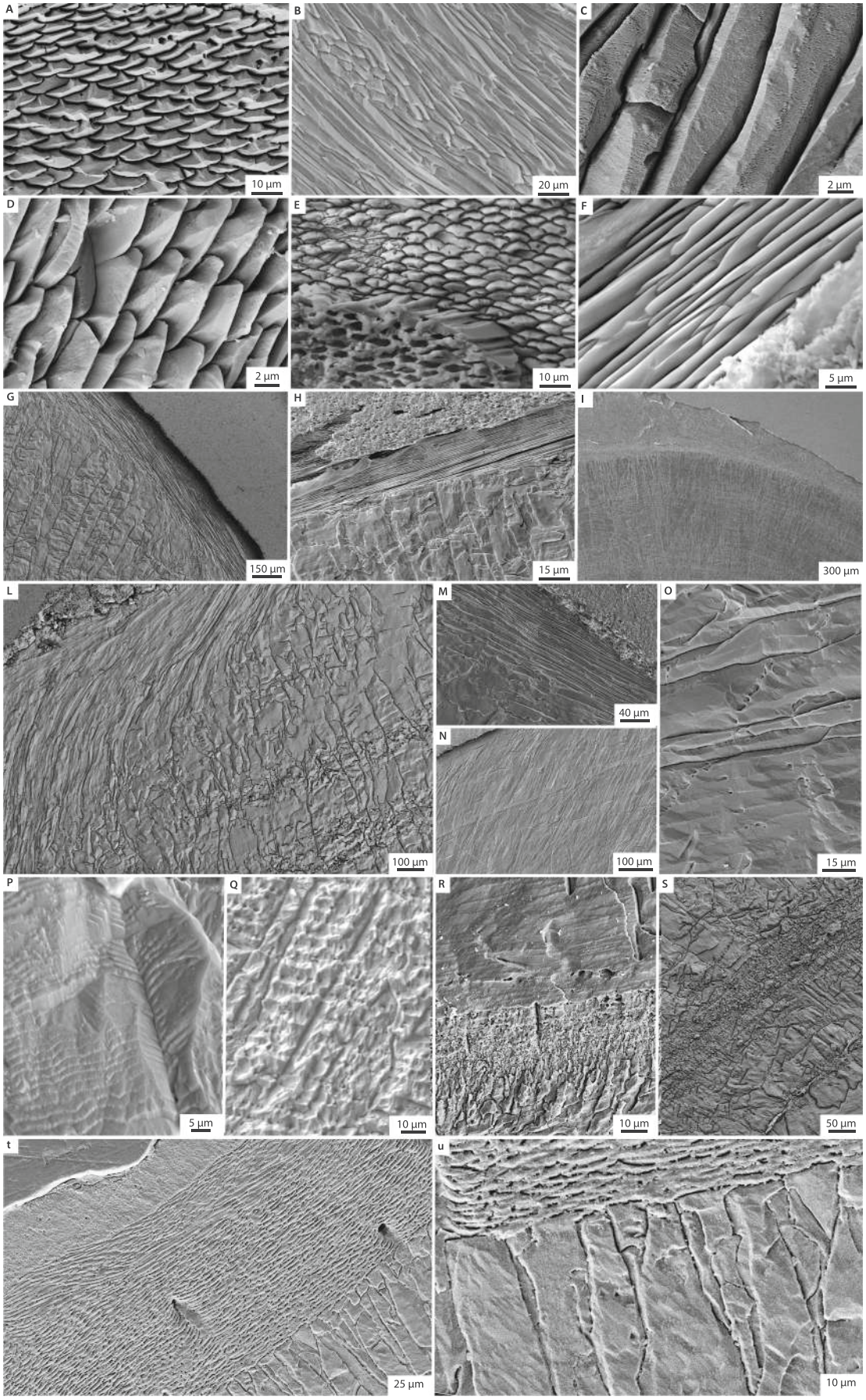

(caption on next page)

Fig. 3. A) Fibers with keel and saddle section, specimen Tri-WH-1 (*Trigonotreta* sp.);
B) fibers in longitudinal view, specimen Tri-WH-2 (*Trigonotreta* sp.); C) details of preserved fibers in B: D) fibers with keel and saddle section, specimen Per-Ju-1 (*Permophricodothyris* sp.); E) fibers with keel and saddle section, specimen Car-WKJ (*Cartorhium* aff. *multiradiatus*); F) fibers in longitudinal view, specimen Mar-WKJ (*Martinia* sp.); G) shell sequence of *Trigonotreta* sp. composed of an outermost fibrous (f) and innermost columnar layer (c), specimen Tri-WH-1; H) shell sequence of *Cartorhium* aff. *multiradiatus* composed of an outermost fibrous (f) and innermost columnar layer, specimen Car-WKJ; L) gradual replacement of columns by fibers in the middle-anterior shell in *Trigonotreta* sp., specimens Tri-WH-1; M) fibers forming an angle of ~13° with the shell surface, specimen Tri-WH-1 (*Trigonotreta* sp.); N) fibers forming an angle of ~40° with the shell surface, specimen Tri-WH-1 (*Trigonotreta* sp.); O) detail of N with fibers showing amalgamation; P) details of columnar layer with accretionary bands, specimen Mar-WKJ (*Martinia* sp.) Q) columnar layer with coarse surface, specimen Com-Bel-1 (*Comelicania* sp.); R) innermost shell showing a porous and coarse microstructure, specimen Tri-WH-1 (*Trigonotreta* sp.); S) contact between the columnar layer and the dental plate, specimen Tri-Ww (*Trigonotreta* sp.).

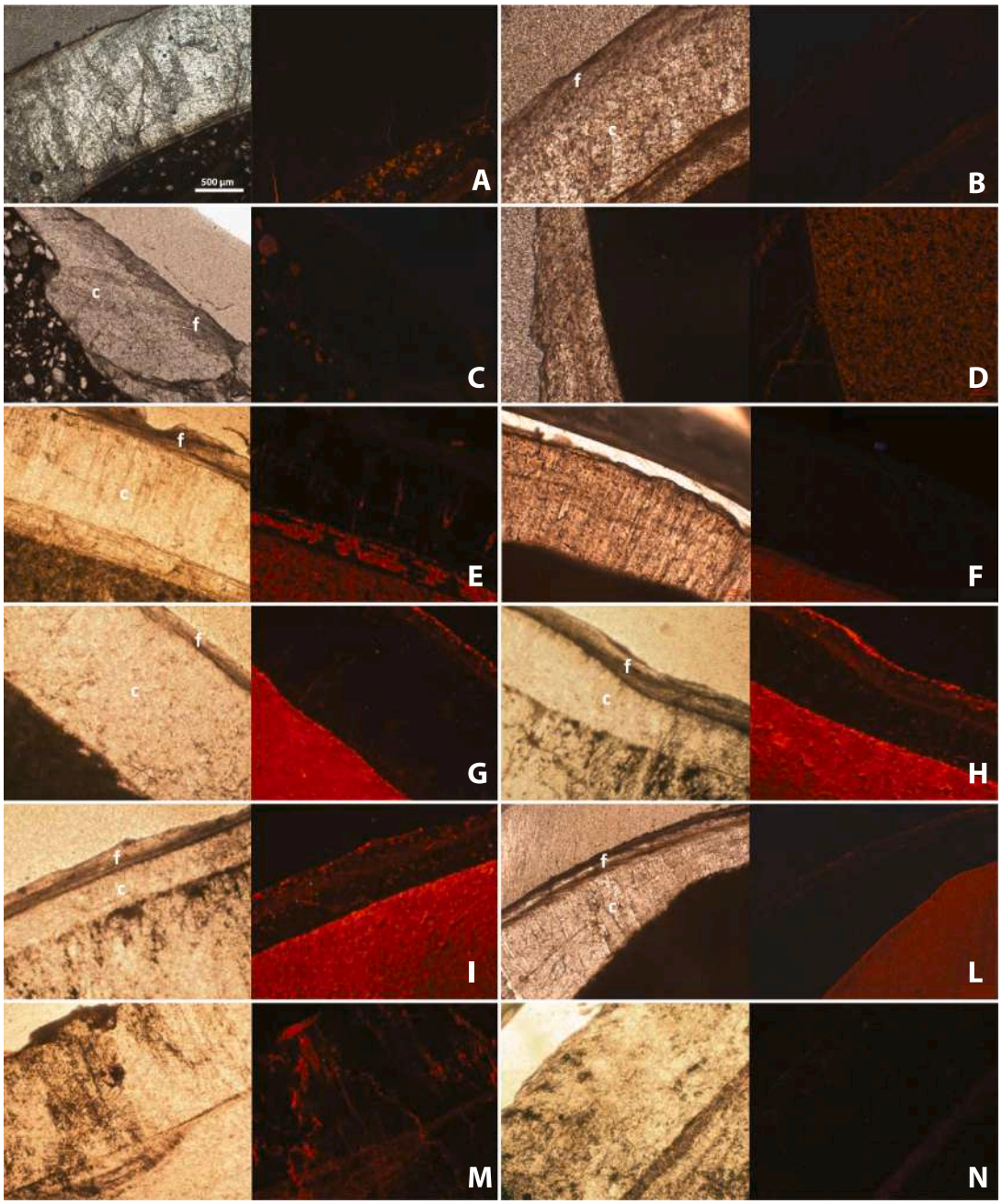

Fig. 4. Luminescence features of the brachiopods specimens under investigation; Images captured with the CL (right) are coupled with optical photomicrographs under transmitted light (left); A) Tri-WH-1 (*Trigonotreta* sp.); B) Tri-WH-2 (*Trigonotreta* sp.); C) Tri-Ww (*Trigonotreta* sp.); D) Ing-Ww (*Ingelarella* sp.); E) Car-WKJ (*Cartorhium* aff. *multiradiatus*); F) Mar-WKJ (*Martinia* sp.); G) Per-Ju-1 (*Permophricodothyris* sp.); H and I) Per-Ju-2 (*Permophricodothyris* sp.); L) Ara-Ju (*Araxathyris* sp.); M) Com-Bel-1 (*Comelicania* sp.); N) Com-Bel-2 (*Comelicania* sp.). Scale bar in Fig. 4A applies to all the images.

revealed that the columnar layer is non-luminescent in most of its portions, (Fig. 4), with slightly bright patches observed in localized regions of some specimens. The fibrous layer can be slightly more luminescent than the columnar, but not always (compare Figs. 4G-H-I-L with Figs. 4B-C). The specimen of *Cartorhium* aff. *multiradiatus* (Car-WKJ) shows luminescent patches in the innermost part of the shell coupled with sporadic luminescence at the boundaries between columns (Fig. 4E). The other specimen from Oman (*Martinia* sp., Mar-WKJ) does not show any relevant luminescence (Fig. 4F), even if the SEM analyses pinpoint signs of localized alteration (Fig. S3). The two specimens belonging the genera *Comelicania* sp. show different pattern of luminescence, with Com-Bel-1 showing luminescent areas (Fig. 4M); while the specimen Com-Bel-2 is non luminescent (Fig. 4N).

The Supplementary and Appendix A contain a description of the stereo-microscope observations and detailed information of each sample. We judged as 'preserved' those samples that fulfill all screening tests using SEM, CL and stereomicroscope, and 'altered' those where one or more of the screening tests was only partially fulfilled or missed.

3.1.2. Minor and Trace elemental (Mg, Fe, Mn, Sr) composition

Trigonotreta sp. (Tri-WH-1) from the Wasp Head Formation, shows both preserved and altered samples, separately clustered, with the altered ones having the highest values for Mn (> 150 ppm), Fe (> 942 ppm), and Mg (> 915 ppm). On the other hand, Sr values remain in the same range for the two groups (795 ppm < Sr < 1288 ppm). The specimens of *Ingelarella* sp. (Ing-Ww) and *Trigonotreta* sp. (Tri-Ww) of the Wandrawandian Siltstone returned similar results to the specimens from the Wasp Head Formation, but a slightly higher degree of correlation between Mn and Fe concentrations is observed. The samples of specimens from the Qarari Unit, *Cartorhium* aff. *multiradiatus* (Car-WKJ) and *Martinia* sp. (Mar-WKJ) have been collected in shell portions deemed to be preserved, avoiding the silicified parts. These samples have concentrations of Mn < 65 ppm and Fe < 180 ppm. Sr has a narrow range comprised between 312 and 421 ppm, the Mg is 350–757 ppm, with one value reaching 1257 ppm, coupled to the highest level of Fe, which equals to 180 ppm.

There is a certain degree of overlap in the TE values of samples deemed preserved and those altered in *Permophricodothyris* sp. (Per-Ju-1 and 2) and *Araxathyris* sp. (Ara-Ju) from the Julfa Formation. Noteworthy, samples judged as altered (see Supplementary S1) bear a relatively low amount of Fe and Mn, well below 100 ppm, but the concentration of Mn seems skewed to slightly higher values (Mn >18 ppm) if compared to the preserved ones (6 ppm < Mn < 19 ppm). Also, Mg and Sr concentrations are very similar to those measured in samples deemed 'preserved'; indeed, altered samples are only slightly more enriched in Sr (306 pp. < Sr < 353 ppm) than the preserved ones (223 pp. < Sr < 321 ppm).

Considering Fe and Mn concentrations, the specimens of *Comelicania* sp. from the Bellerophon Formation show separate clusters for preserved samples (Fe ranges 26–39 ppm, Mn ranges 4–8 ppm) and altered ones (Fe ranges 43–428 ppm, Mn ranges 9–156 ppm). Com-Bel-1 shows a high correlation between Fe and Mn, and a higher concentration of these elements. A certain degree of overlap is observed for Mg and Sr in altered and preserved samples, but Sr has concentrations skewed to lower values in altered (381 ppm < Sr < 547 ppm) than in preserved ones (530 ppm < Sr < 580 ppm) (Table 2, Figs. S4, S5).

3.2. $\delta^{13}C$ and $\delta^{18}O$ values of the columnar layer and their ontogenetic time series

3.2.1. Cross plots of $\delta^{13}C$ versus $\delta^{18}O$ values

The $\delta^{18}O$-$\delta^{13}C$ values cross plots (Fig. 5) and Table S1 summarize the results of the isotopic analyses. In most of the analyzed specimens, altered samples have low $\delta^{13}C$ and $\delta^{18}O$, but exceptions are present. Indeed, the altered samples of *Comelicania* sp. (Com-Bel-1) show the highest coefficients of correlation and r^2 between $\delta^{13}C$ and $\delta^{18}O$ values ($r^2 = 0.76$), supported by highly significant *P*-values (<0.001, Table S1), with the values strongly clustered around a regression line showing a positive slope.

Considering only the well preserved samples collected from the columnar layer of nearly all analyzed species, $\delta^{18}O$ and $\delta^{13}C$ values are significantly correlated, with an r^2 ranging from 0.09 to 0.61 (Table S1). The specimens Car-WKJ and Lio-DS show low significant values with the r^2 equal to 0.004 and 0.03 respectively. The slope of the regression line is negative in the specimens Tri-WH-2 and Ara-Ju, but in all other cases it is positive, with differences in the absolute value of the slope. The ranges of observed values exceed 2‰ for both isotopes in Tri-WH-1 and 2; instead, they are narrower in Tri-Ww and Ing-Ww. Per-Ju-1, Per JU-2, Ara-Ju, Car-WKJ, Mar-WKJ, Com-Bel-2 and Lio-DS show $\delta^{18}O$ values somewhat clustered and comprised in a range of <1.00‰, and the $\delta^{13}C$ values in a range of ~1.5‰.

3.2.2. $\delta^{18}O$ profiles

The specimens Tri-WH-1 and 2 show clear $\delta^{18}O$ values variations along the growth axis, with the oscillation range exceeding 2.0‰ units. Anteriorly along the longitudinal axis, there is a reduction in the amplitude of the oscillations, coupled with a trend towards more positive $\delta^{18}O$ values (Figs. 6A-B). The transects obtained from Tri-Ww and Ing-Ww show more irregular variations along the shell length, with the amplitude of $\delta^{18}O$ values exceeding 0.5‰ in some parts of the shell (Figs. 7A-B), also observed in the specimens Car-WKJ and Mar-WKJ (Figs. 7C-D). In these specimens, the $\delta^{18}O$ values become more

Table 2
Summary of the trace element composition of samples.

Specimen	Samples	Mg [ppm]		Sr [ppm]		Fe [ppm]		Mn [ppm]	
		min	Max	Min	max	min	max	min	max
Tri-WH-1	Preserved	658	931	997	1099	141	177	17	25
	Altered	897	2318	915	1084	942	1187	151	197
Tri-WH-2	Preserved	549	835	795	1288	51	203	8	31
Tri-Ww	Preserved	528	612	721	792	33	58	9	36
	Altered	535	1276	614	738	215	8769	216	2234
Ing-Ww	Preserved	352	444	701	763	13	32	4	36
	Altered	361	412	656	690	19	48	6	35
Mar-WKJ	Preserved	350	550	312	360	6	49	0.5	65
Car-WKJ	Preserved	469	1279	339	412	24	180	14	65
Per-Ju-1	Preserved	785	941	223	261	45	101	15	19
	Alterd	797	797	306	306	49	49	21	21
Per-Ju-2	Preserved	838	1364	269	321	43	141	9	16
	Altered	1157	1505	328	359	59	102	18	25
Ara-Ju	Preserved	668	757	292	298	33	44	6	14
Com-Bel-1	Altered	822	1464	381	545	103	428	40	156
Com-Bel-2	Preserved	1107	1926	530	590	26	39	4	8
	Altered	1067	1430	497	547	43	142	9	14

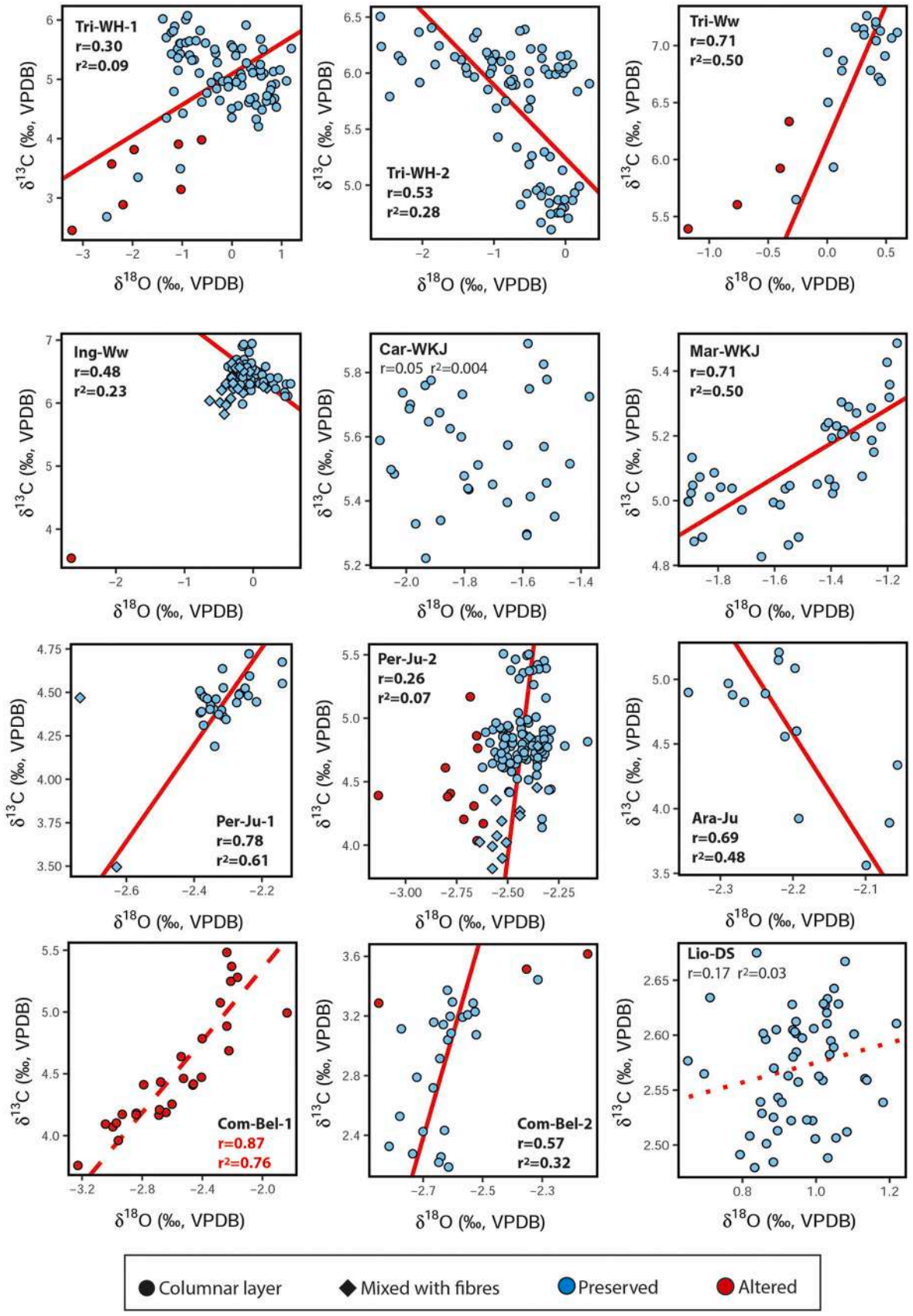

Fig. 5. Cross plots of shell $\delta^{18}O$ and $\delta^{13}C$ values of the samples. Circles and diamonds represent samples from the columnar layer and those contaminated by sampling of fibrous layer; Cyan color represents samples deemed to be preserved, and red are altered samples. The regression line, r, and r^2 are calculated for preserved samples of the columnar layer; in the specimen Com-Bel-1 the calculation refers to altered samples. (For interpretation of the references to color in this figure legend, the reader is referred to the web version of this article.)

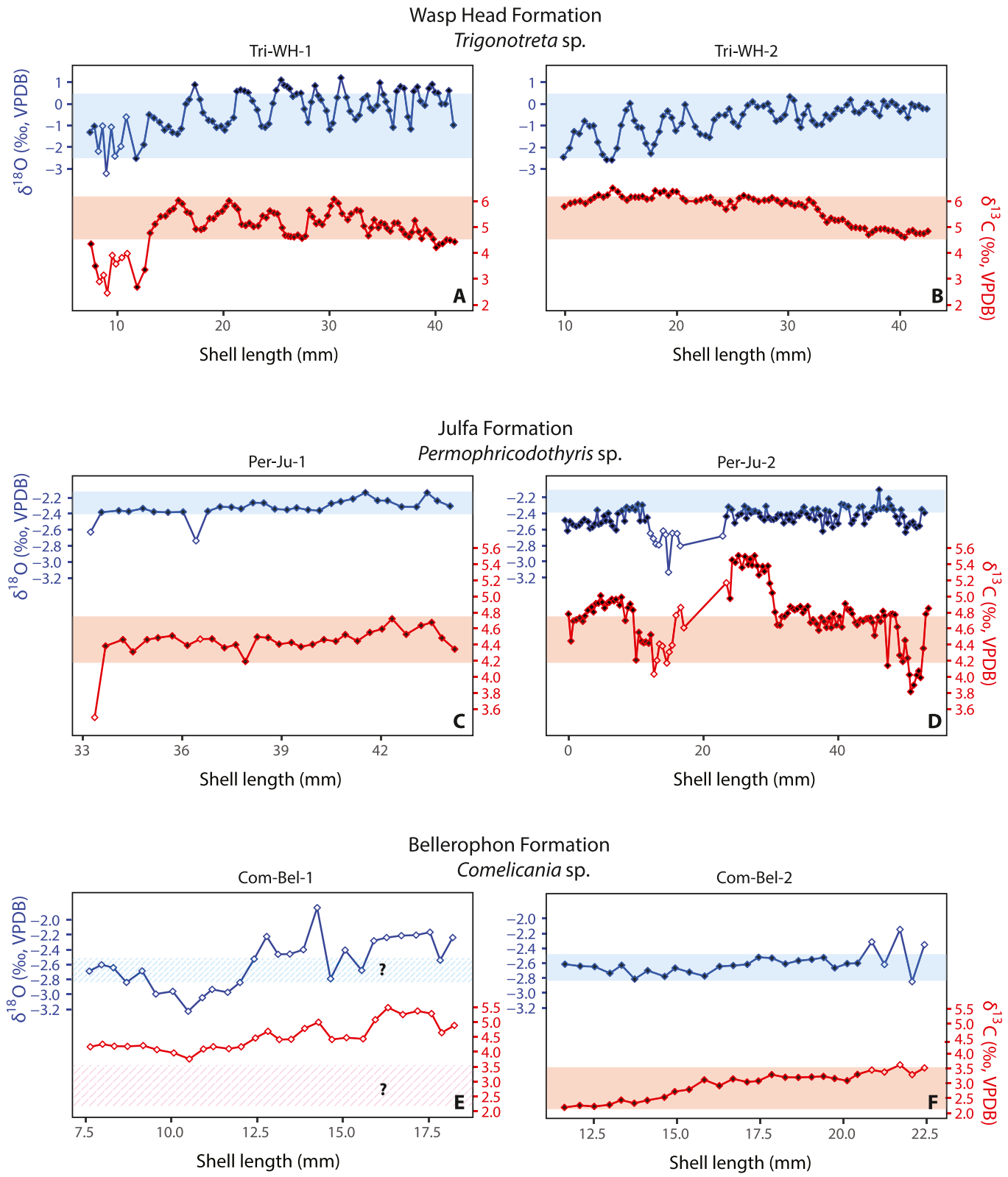

Fig. 6. Intra-generic comparison of profiles of the $\delta^{18}O$ (blue color) and $\delta^{13}C$ (red color) along the mid-shell longitudinal section for the different specimens; open diamonds represent samples deemed to be altered based on the screening test; the shadow blue and red areas represent the range of overlap between specimens collected at the same localities; for the Dolomites samples, the shadow areas represent the range of the preserved specimen Com-Bel-1. The direction of shell growth is from left to right in each panel. (For interpretation of the references to color in this figure legend, the reader is referred to the web version of this article.)

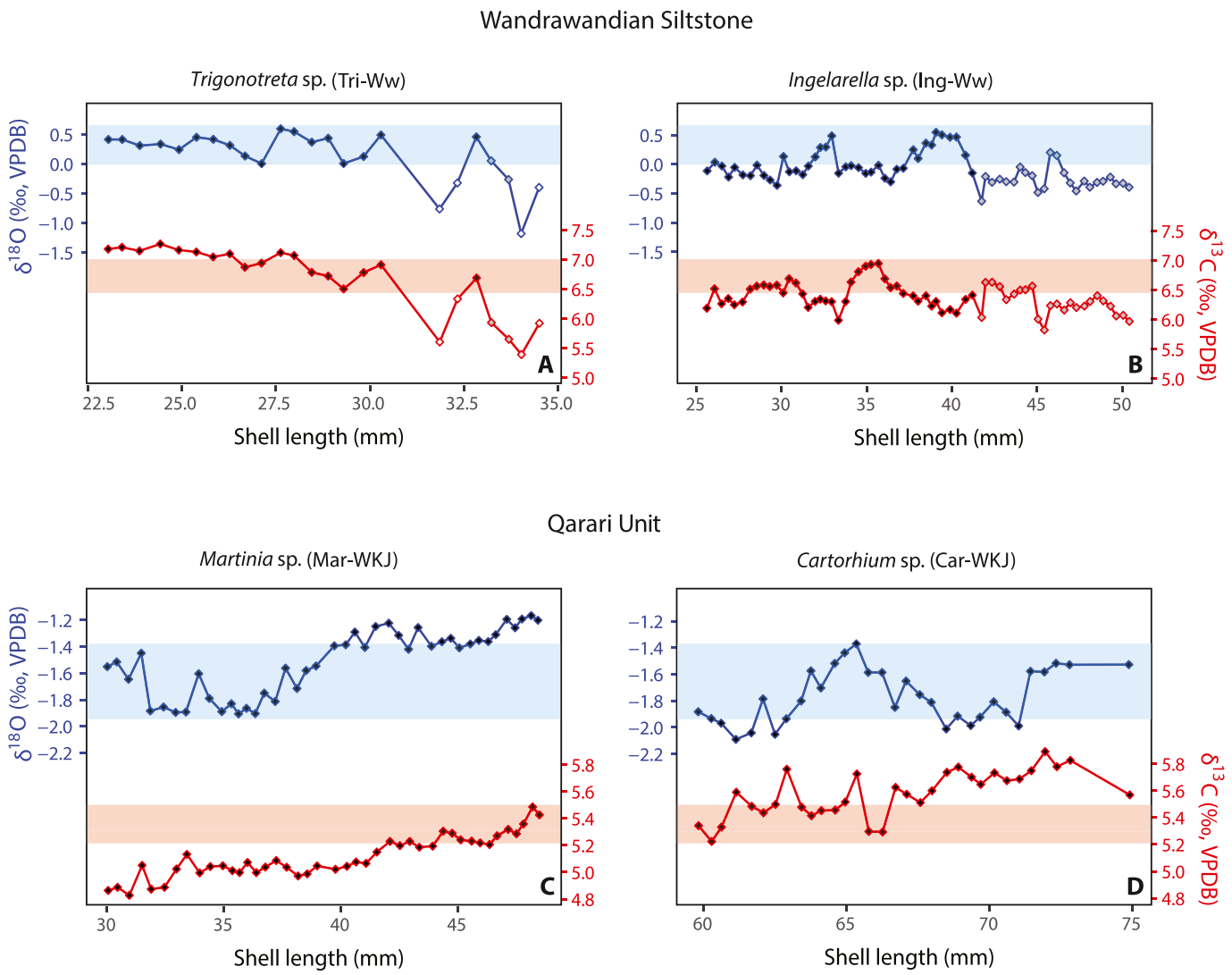

Fig. 7. Inter-generic comparison of profiles of the $\delta^{18}O$ (blue color) and $\delta^{13}C$ (red color) values along the mid-shell longitudinal section for the different specimens; open diamonds represent samples deemed to be altered based on screening test; gray diamonds represent samples where the columnar layer is contaminated by fibrous layer; the shadow blue and red areas represent the range of overlap between specimens of the same species collected at the same localities. (For interpretation of the references to color in this figure legend, the reader is referred to the web version of this article.)

positive towards the anterior margin. In Per-Ju-1 and 2, the $\delta^{18}O$ values are steady throughout the longitudinal profiles, remaining around mean values of −2.3 to −2.4‰, with no distinct oscillations and a range excursion of more than ~0.2‰ (Figs. 6C-D). Slightly higher $\delta^{18}O$ values are recorded towards the anterior margin. At the same locality, Ara-Ju shows a similar range of variation around a mean value of 2.2‰, with higher values anteriorly (Fig. 9). Com-Bel-2 shows steady $\delta^{18}O$ values with a weak irregular oscillation around the mean values −2.6‰ (Fig. 6F). For what concerns the altered specimen, Com-Bel-1 shows $\delta^{18}O$ values in a range of variation of ~1‰ (Fig. 6E). The profile of $\delta^{18}O$ in Lio-DS has some variation within a range equal to ~0.6 ‰, around a mean value of ~1‰ (Fig. 8). Table 3 summarizes the mean and variance of $\delta^{18}O$ values, measured along the longitudinal axis.

3.2.3. *Profile of $\delta^{13}C$ measurements*

Excluding a few values from the posterior region of Tri-WH-1, the specimens of *Trigonotreta* sp. from the Wasp Head Formation show a range of $\delta^{13}C$ values between +4.2‰ and +6.5‰ (Figs. 6A-B). In Tri-WH-1, the oscillations of $\delta^{13}C$ values are evident, but become damped in the anterior part of the shell, where the isotope values become lower than in the posterior region. The profile of Tri-WH-1 is flat, it shows weak oscillations, and there is a trend towards lower $\delta^{13}C$ values towards the anterior margin. The profile of Tri-Ww has a similar trend to Tri-WH-1, with values varying from +5.4‰ to +7.3‰. Ing-Ww shows a variation from +6.0‰ to +6.9‰. The profiles of specimens from the Wandrawandian Siltstone (Tri-Ww and Ing-Ww) record some evident fluctuations, which are not regular (Figs. 7A-B).

$\delta^{13}C$ values in the profiles of *Martinia* sp. (Mar-WKJ) and *Cartorhium* aff. *multiradiatus* (Car-WKJ) range from +4.8‰ to +5.5‰ and from +5.2‰ to +5.9 ‰, respectively. These specimens show a trend of increasing $\delta^{13}C$ values towards the anterior margin, with fluctuations in the range of 0.3‰ (Figs. 7C-D).

The specimens from the Julfa Formation show profiles within a narrow range of variability (Figs. 6C-D). Per-Ju-2 shows $\delta^{13}C$ values between +4.5‰ and +5.0‰ in the first part of the shell length, with minor fluctuations. At about 23 mm of the shell length, the $\delta^{13}C$ values increases to +5.4‰. In the anteriormost part, at about 49 mm of the shell length, values drop to +3.8‰. The profile of Per-Jul-1 is steady with values between +4.3‰ and +4.7‰, with an outlier value of +3.5‰ recorded in a sample of columnar layer contaminated by fibers. Ara-Ju shows values decreasing from +5‰ posteriorly to +3.5‰ anteriorly (Fig. 9). The profile of Com-Bel-2 does not show any oscillation but an

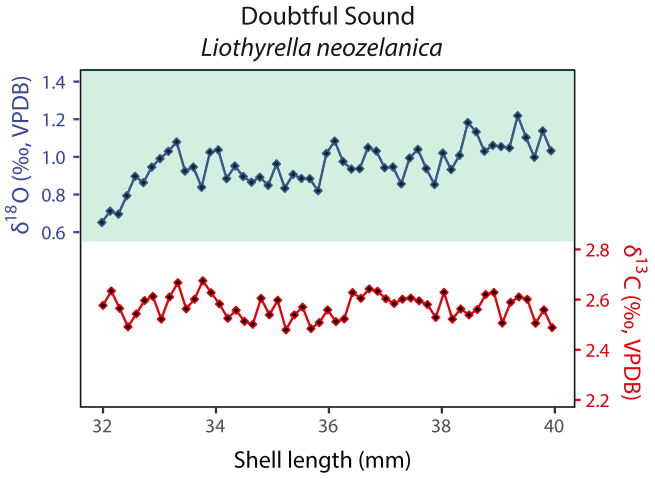

Fig. 8. Profiles of the $\delta^{18}O$ (blue color) and $\delta^{13}C$ (red color) along the mid-shell longitudinal section for the recent *Liothyrella neozelanica* collected in Doubtful Sound, New Zealand. The shaded area represents the possible range values of equilibrium calcite at the locality of collection ($\delta^{18}O_{eq\text{-}cal}$ range = 0.5–1.8 ‰), calculated with the equation of Watkins et al. (2014) and using the ranges of temperatures from Goodwin and Cornelisen (2012). The $\delta^{18}O$ for seawater is estimated with the equation $\delta^{18}O_{sw}$ = 0.39 * Salinity - 13.46 (Brand et al., 2013) using the ranges of salinity measured in Gibbs et al. (2000). (For interpretation of the references to color in this figure legend, the reader is referred to the web version of this article.)

increasing trend of the $\delta^{13}C$ values, from ~ +2.2‰ to ~ +3.4‰ (Fig. 6F).

The $\delta^{13}C$ values of the altered specimens become higher anteriorly. Com-Bel-1 spans from +3.8‰ to +5.5‰. The profile of $\delta^{13}C$ in Lio-DS is rather stable around the mean value of +2.6‰, with a range of variation spanning from +2.5 to +2.7‰ (Fig. 8).

3.3. Statistical analyses

The cluster analysis highlights that about 8% of the samples were misplaced, i.e. judged as potentially preserved combining SEM, CL and optical screening, but included in the altered cluster based on elemental values (see paragraph 2.4; Supplementary, Fig. S6). The combined use of the SEM, CL and optical evaluation has led to an appropriate evaluation in terms of preservation vs alteration of the majority of the samples (>90%) in this specific study.

In most cases, the altered samples show lower isotope values than the preserved ones (Table 2). The specimen Com-Bel-2 represents an exception since the altered samples fall in the upper ranges of $\delta^{13}C$ and $\delta^{18}O$ values. The linear models indicate that, in most specimens, the oxygen isotopic composition depends on the position of the sample along the shell length transect, with the values becoming increasingly higher along the growth direction (Table 4). Exceptions are present in the specimens Car-WKJ and Tri-Ww, where the models show an insignificant *p*-value or even decreasing $\delta^{18}O$ values towards the anterior margin. The skewness of the residuals of linear models has mostly negative values for samples collected in the Sydney Basin whereas positive for other localities, even if there are exceptions. The confidence

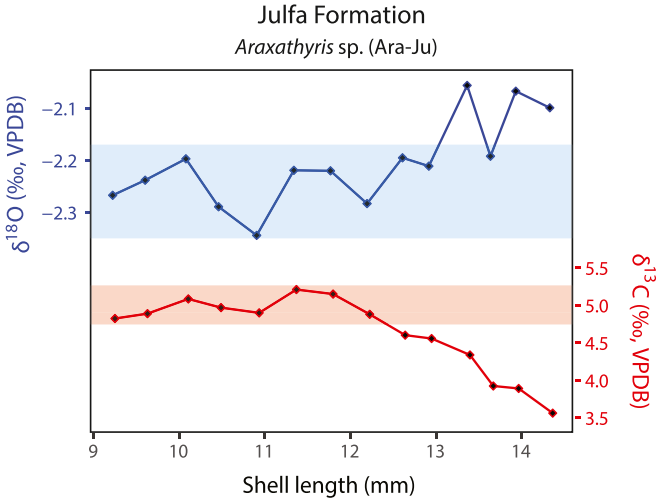

Fig. 9. Profiles of $\delta^{18}O$ (blue color) and $\delta^{13}C$ (red color) values along the mid-shell longitudinal section of the athyrididе *Araxathyris* sp. (Ara-Ju); the shadow blue and red areas represent the range of overlap with the specimens of species of the spiriferide *Permophricodothyris* (Per-Ju-1 and 2) collected in the same locality. (For interpretation of the references to color in this figure legend, the reader is referred to the web version of this article.)

Table 3
Mean, standard deviation (sd) and variance of $\delta^{18}O$ and $\delta^{13}C$ values of the different samples in each specimen under investigation; * only a single value is available.

		$\delta^{18}O$			$\delta^{13}C$			
Specimen	Samples	Mean	Sd	Variance	Mean	Sd	Variance	N
TRI-WH-1	Columnar preserved	−0.2	0.09	0.62	5.1	0.1	0.3	84
	Columnar altered	−1.8	0.35	0.85	3.4	0.2	0.3	7
TRI-WH-2	Columnar preserved	−0.7	0.08	0.50	5.7	0.1	0.3	83
Tri-Ww	Columnar preserved	0.3	0.04	0.03	7.0	0.05	0.05	18
	Columnar altered	−0.7	0.20	0.15	5.8	0.20	0.17	4
	Mixed with fibers	−0.1	0.16	0.05	5.8	0.14	0.04	3
Ing-Ww	Columnar preserved	0.0	0.04	0.06	6.4	0.04	0.05	41
	Columnar altered	−2.6			3.5			1
	Mixed with fibers	−0.3	0.04	0.03	6.3	0.04	0.05	24
Mar-WKJ	Columnar preserved	−1.5	0.04	0.06	5.1	0.02	0.02	43
Car-WKJ	Columnar preserved	−1.8	0.04	0.04	5.6	0.03	0.03	32
Per-Ju-1	Columnar preserved	−2.3	0.01	0.00	4.5	0.02	0.01	29
	Mixed with fibers	−2.7	0.05	0.01	4.0	0.49	0.47	2
Per-Ju-2	Columnar preserved	−2.4	0.01	0.01	4.8	0.03	0.08	99
	Columnar altered	−2.7	0.04	0.02	4.5	0.10	0.11	11
	Mixed with fibers	−2.5	0.03	0.01	4.2	0.09	0.10	13
Ara-Ju	Columnar preserved	−2.2	0.02	0.01	4.6	0.14	0.26	14
Com-Bel-1	Columnar altered	−2.6	0.06	0.11	4.5	0.09	0.21	28
Com-Bel-2	Columnar preserved	−2.6	0.02	0.01	2.9	0.08	0.17	25
	Columnar altered	−2.4	0.21	0.13	3.5	0.10	0.03	3
Lio-DS	Columnar (preserved)	1.0	0.01	0.01	2.6	0.01	0.002	55

Table 4
Parameters of two different linear models to test if there is a significant effect of the shell length on the $\delta^{18}O$ values. The first is a linear model between the sample position on the shell length and $\delta^{18}O$ values. The second is a model between the sample position on the shell length and the residue of IMFs using the Hilbert Huang transform. Values marked with (*) indicate samples that show no significant effect or where the correlation is negative; all the other values are highly significant and highlight a positive correlation between the shell position and the $\delta^{18}O$ value; β and β_1 are the coefficients of the linear models alongside their significant values; r^2 is the r-squared of each model.

Linear Model	Specimen	β	p-value	β_1	p-value	r^2	p-value
$\delta^{18}O \sim$ Shell length	**Tri-WH-1**	−1.30	<0.0011	0.042	<0.001	0.22	<0.001
	Tri-WH-2	−2.05	<0.001	0.050	<0.001	0.46	<0.001
	Tri-Ww	0.36*	0.43*	−0.001*	0.97*	−0.06*	0.97*
	Ing-Ww	−0.87	<0.001	0.027	<0.001	0.23	<0.001
	Mar-WKJ	−2.88	<0.001	0.034	<0.001	0.60	<0.001
	Car-WKJ	−2.90	<0.001	0.017*	0.05*	0.09*	0.05*
	Per-Ju-1	−2.88	<0.001	0.015	<0.001	0.44	<0.001
	Per-Ju-2	−2.49	<0.001	0.0013	<0.001	0.17	<0.001
	Ara-Ju	−2.62	<0.001	0.035	0.01	0.44	0.01
	Com-Bel-2	−2.95	<0.001	0.019	<0.001	0.29	<0.001
	Lio-DS	0.83	<0.001	0.031	<0.001	0.39	<0.001
$\delta^{18}O \sim$ Shell length after removing higher frquency signal using the Hilbert Huang Transform	**Tri-WH-1**	−1.37	<0.001	0.044	<0.001	0.56	<0.001
	Tri-WH-2	−1.95	<0.001	0.047	<0.001	0.85	<0.001
	Tri-Ww	0.54	<0.001	−0.009	<0.001	0.52	<0.001
	Ing-Ww	−0.80	<0.001	0.024	<0.001	0.44	<0.001
	Mar-WKJ	−3.01	<0.001	0.038	<0.001	0.79	<0.001
	Car-WKJ	−0.90	0.02	−0.012*	0.04*	0.11*	0.04*
	Per-Ju-1	−2.82	<0.001	0.013	<0.001	0.98	<0.001
	Per-Ju-2	−2.48	<0.001	0.002	<0.001	0.33	<0.001
	Ara-Ju	−2.59	<0.001	0.031	<0.001	0.87	<0.001
	Com-Bel-2	−3.00	<0.001	0.022	<0.001	0.74	<0.001
	Lio-DS	−0.03*	0.123*	0.01*	0.137*	0.05*	0.136*

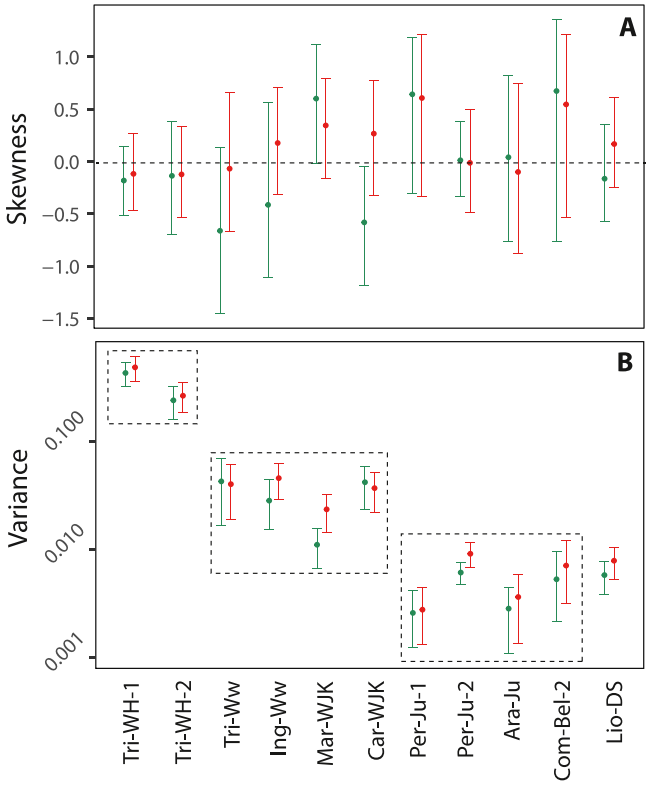

Fig. 10. Skewness (A) and variance (B) of the residuals from the linear model between $\delta^{18}O$ values and shell length (red) and of the time series de-trended using the residual of the signal decomposition after the Huang-Hilbert transform (green). (For interpretation of the references to color in this figure legend, the reader is referred to the web version of this article.)

intervals show a certain amount of overlap between the specimens (Fig. 10A). The variance of residuals shows significant variations between localities and time intervals, of different orders of magnitude (Fig. 10B). The Lopingian shell samples, from the Julfa and Bellerophon formations, present the lowest value of $\delta^{18}O$ variance along the longitudinal axis. The samples from the Wasp Head Formation show the greatest variance. The samples from the Wandrawandian Siltstone and the Qarari Unit have a similar variance. The modern specimen from Doubtful Sound (New Zealand) shows a variance value in the range of that expected for inorganic calcite precipitated in equilibrium at the site of collection (green field in Fig. 8). The variability of variance among specimens and localities returns differences in the amplitude of the oscillatory signal, after removing the trend related to the correlation between $\delta^{18}O$ values and the position along the shell length transect. The two different approaches, i.e. the residuals of the regression model and the residue of the Intrinsic Mode Functions, show a straightforward similarity (Fig. 11).

4. Discussion

4.1. Evaluation of diagenetic alteration

In this study, the samples deemed 'altered' based on SEM, CL, and optical analyses have the highest concentrations of Mn and Fe. However, some studies reported comparatively low Mn contents in partially altered brachiopods, suggesting that a low amount of this element may not always be indicative of good preservation (Harlou et al., 2016).

Enrichment in Mg is also an indicator of poor preservation, as shown by the samples of the Sydney Basin. Indeed, in the specimens from the Wasp Head Formation and Wandrawandian Siltstone, a slight enrichment of Mg seems to be more diagnostic than the depletion of Sr to indicate alteration because it is often coupled with higher values of Fe and Mn (Mii et al., 2012; Garbelli et al., 2019). Formation of authigenic carbonates enriched in Mn, Mg and Fe may occur in reducing conditions of burial during early diagenesis (Ni et al., 2020). In fact, samples with slightly higher Mg and Fe are sampled near regions of the shell affected by microfracture or alteration (see Appendix A).

The evaluation of Sr alone is not straightforward, since the columnar layer has a D_{Sr} overlapping the values of equilibrium calcite (Rollion-Bard et al., 2019) and the alteration may lead either to depletion of Sr (Brand and Veizer, 1980) or to its enrichment (e.g. Fig. 6C in Wang et al., 2021), depending on several factors. For example, since mechanisms of

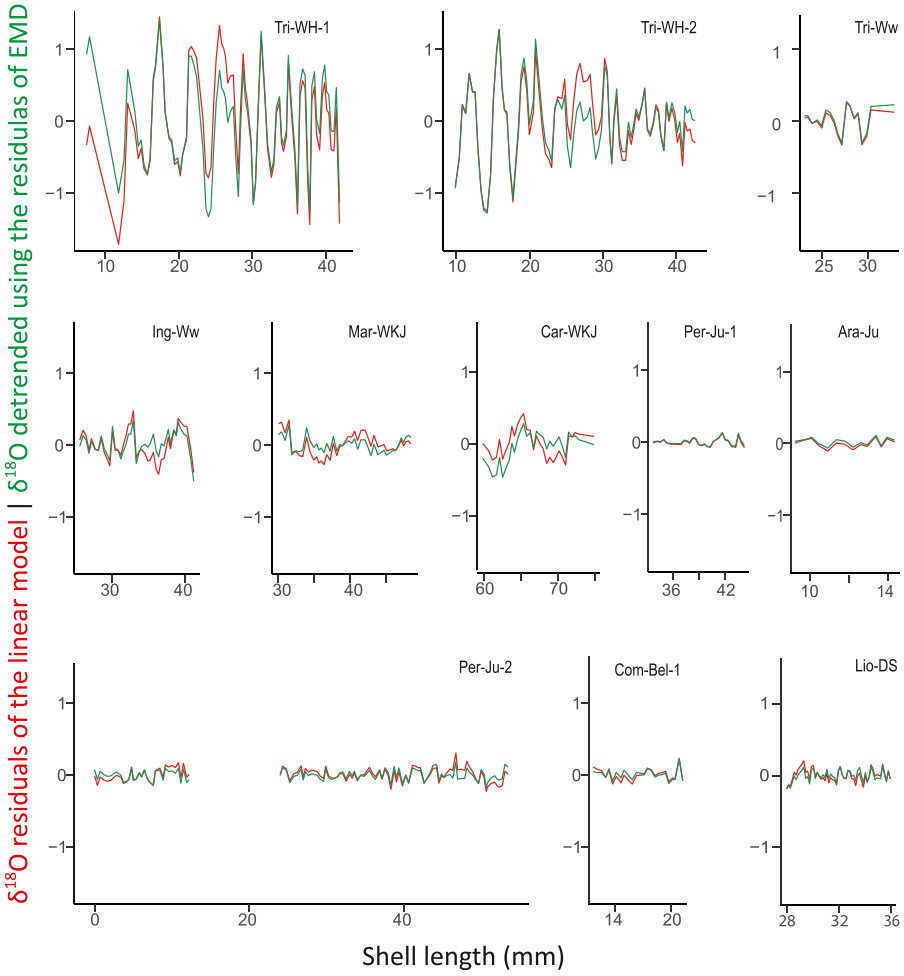

Fig. 11. Amplitude of the oscillatory signal in the specimens after removing the main trend related to the correlation between $\delta^{18}O$ values and shell length using two different approaches; in red the residuals of a regression model between $\delta^{18}O$ values vs the samples position on the shell length are plotted; in green, the residue of the Intrinsic Mode Functions has been removed to the seasonal signal of $\delta^{18}O$ values. (For interpretation of the references to color in this figure legend, the reader is referred to the web version of this article.)

carbonate deposition forming the limestone have a Sr/Ca partition coefficient (D_{Sr}) similar to inorganic precipitation (Krause et al., 2018), sample contamination by the enclosing rocks will not affect distinctly the Sr concentration of the shell, when the limestone preserves the primary composition. In fact, Upper Permian limestones from Iran have ranges of Sr concentrations similar to the columnar layer of the preserved brachiopod shells there enclosed (Garbelli et al., 2012; Schobben et al., 2016). In contrast, the enclosing rock of the specimens of Bellerophon Formation of the Dolomites has no longer a primary composition. Here, samples deemed altered show a depletion of Sr (Brand et al., 2012; Garbelli et al., 2022a). Published data suggests that Sr has commonly low concentration in diagenetic carbonates (Banner, 1995).

Specimens, as those from Oman, characterized by the excellent preservation of the original structural elements, a feature indicative of good shell preservation according to Casella et al. (2018), show a narrow range of variation for the trace elements. They are non-luminescent with relatively low content of Mn and Fe. Considering the partition coefficient of the columnar layer (Rollion-Bard et al., 2019), the Sr concentration of coeval Permian seawater should have been ~4.5± 0.3–6.1 ±0.4 mmol/mol of Sr/Ca, similar to data presented in previous research (Steuber and Veizer, 2002). Moreover, the main process of alteration of these specimens is related to silicification, which appears localized in the fibrous layer. In fact, the decay of organic material between the fibers (Simonet Roda et al., 2019) creates favorable conditions for carbonate dissolution and silica precipitation (Butts and Briggs, 2011). By contrast, the columnar layer has a low content of organic matter; therefore, it is generally less prone to silicification (Fig. S3; Garbelli, 2017), even if this process can involve also the columnar layer as previously observed (Angiolini et al., 2019).

Despite the different diagenetic processes observed in the analyzed material, there is a significant correlation between trace elements and the results of the screening test with SEM, CL, and optical evaluation (Figs. S4, S5). The $\delta^{18}O$ vs $\delta^{13}C$ values cross plots confirm that the screening by multiple techniques of the columnar layer allows to discern preserved material with primary or nearly-primary signal. Altered samples generally cluster apart from preserved ones. In one case, Com-Bel-1 (Fig. 5), the isotopic values are highly correlated, indicating that they may represent a continuum from slight to high diagenetic alteration. In this case, the samples recording lower $\delta^{13}C$ and $\delta^{18}O$ values are those slightly enriched in Fe and Mn.

4.2. *Intra-generic and inter-generic comparison of $\delta^{13}C$ and $\delta^{18}O$ values*

A certain variability of the recorded geochemical proxies is expected even when comparing specimens of the same species from the same stratigraphic position because, due to time averaging, the shells do not cover precisely the same time interval in terms of tens or hundreds of years or more and climate and environmental conditions can vary in a few decades. However, despite the slightly different stratigraphic positions, general trends can be deduced. For example, the specimens of *Trigonotreta* sp., show clear $\delta^{18}O$ values oscillations, and it is evident that the recorded trends are very similar.

The comparison between the two specimens of *Permophricodothyris* sp. indicates that individuals of species of the same genus record a comparable signal, even if in this case, they do not record a clear and regular seasonal variation, probably due to their low latitude location (see 4.5).

Also, the profiles of $\delta^{13}C$ values are comparable to some extent in congeneric species. The specimens of species of *Trigonotreta* and *Permophricodothyris* show similar mean trends.

The different degrees of co-variation between the $\delta^{13}C$ and $\delta^{18}O$ and in the sign and slope of the regression line of cross plots suggests that kinetic fractionation alone does not explain the distribution of isotope ratios values. The increase of r^2 values after removing the higher frequency signal in the computation of the $\delta^{18}O \sim$ samples position along the shell length models coupled with a positive slope in most of the specimens, suggests the presence of effect related to change in the growth during the ontogeny (Table 4). Thus, the effect of growth rate has to be taken in account when evaluating the isotopic composition of fossils brachiopods shells, as observed in modern species (Yamamoto et al., 2010, 2013; Takayanagi et al., 2015).

The comparison of the $\delta^{18}O$ values in species of different genera from the same locality shows that the ranges of values widely overlap in the taxa belonging to the Spiriferida (Fig. 7). Specimens of *Ingelarella* sp. and *Trigonotreta* sp. from Australia show a very similar range of $\delta^{18}O$ values. The same holds true for the specimens of *Cartorhium* aff. *multiradiatus* and *Martinia* sp. from Oman. In both cases of the specimens from Australia and Oman, the comparison involved shells belonging to species of different genera, and also to separate families, i.e. the Trigonotretidae and Ingelarellidae in the first case, and the Brachythyrididae and Martiniidae in the second.

The mean and variance are similar for the columnar layer of different spiriferid genera collected in the same localities and paleolatitudes, suggesting that the incorporation mechanism of oxygen isotopes is similar among the members of this order.

The intergeneric comparison of the $\delta^{13}C$ values profiles reveals that the values partially overlap. When the comparison is extended to taxa of different orders from the same locality, as for instance between *Araxathyris* sp. (Athyridida) and *Permophricodothyris* sp. (Spiriferida) from Iran, it is shown that both the $\delta^{18}O$ and $\delta^{13}C$ values partially overlap and that the statistical parameters are similar.

A common pattern seems present in specimens from different time intervals and environment and taxa. After purging the signal from short term perturbations (i.e. to those due to seasonality or shorter process), a trend of increasing $\delta^{18}O$ values, coupled with $\delta^{13}C$ ones, is present in the middle-posterior region of the shell. Towards the anterior margin, the $\delta^{13}C$ values begin to decrease, while $\delta^{18}O$ values continuously increase, but more slowly.

4.3. Quality of the columnar layer archive

Studies on living species of *Liothyrella neozelanica* Thomson, 1918 and *Gryphus vitreus* (Born, 1778) revealed that portions of the columnar layer show $\delta^{18}O$ variations that are in agreement with the range of temperature and salinity variations of the surrounding environment (Rollion-Bard et al., 2019). The $\delta^{18}O$ profile of Lio-DS well agrees with the former results since we observed a variation of ~0.6 ‰, corresponding to a range of temperature variation equal to ~3 °C at depth ~18 m in Deep Cove at Doubtful Sound. Here temperatures recorded over the five-year period March 2005 to March 2010 return a 99th interpercentile range equal to 4.2 °C (Goodwin and Cornelisen, 2012). Therefore, the use of this archive for seasonal paleotemperature reconstructions is highly attractive because it can return reliable estimate of intra-annual temperature variation and numerous taxa develop this layer during the Paleozoic (Angiolini, 1993; Angiolini et al., 2012, 2019; Garbelli, 2017; Garbelli et al., 2014).

The trends observed in the studied specimens of *Permophricodothyris* sp. and *Trigonotreta* sp. indicate similarities in the rate of shell accretion, as observed in recent analogues (Takayanagi et al., 2015), and in the geochemical composition of the columnar layer. These specimens record higher $\delta^{18}O$ values in the anterior part of the shell (the last secreted calcite, Fig. 6). Therefore, after a higher growth rate in the juvenile stage, characterized by a wider range of $\delta^{18}O$ values in the shell calcite, the rates of deposition of the columnar layer decrease, and records a narrower range of $\delta^{18}O$, skewed to higher values.

Superimposed on this trend, is the occurrence of more or less regular oscillations of $\delta^{18}O$ and $\delta^{13}C$ values along the growth transect, and a decrease in their amplitude towards the anterior margin (e.g. *Trigonotreta* sp., Tri-WH-1 and 2). This is comparable to the trend observed in the recent *Terebratulina crossei* Davidson, 1882 (Takayanagi et al., 2015), suggesting a time-averaging effect due to the reduced growth rates with age. Moreover, during the late phases of the growth, an enrichment in ^{12}C has been observed, probably derived by metabolic activity, possibly related to the individual becoming mature and spawning (Takayanagi et al., 2015).

The low r^2 coefficients of $\delta^{18}O$ and $\delta^{13}C$ values measured in Lio-DS (Fig. 5) suggest that the variations in the columnar layer seem not to be controlled by kinetic fractionation as previously indicated by Rollion-Bard et al. (2019). The correspondence between the positive peaks of $\delta^{18}O$ values and the negative ones of $\delta^{13}C$ values in *Trigonotreta* sp. Tri-WH-1, and also, even if less evident, in the specimen Tri-WH-2, suggests that these oscillations were related, at least in part, to temperature and environmental changes of the cold water settings where these brachiopods lived. Although, an increase in temperature prompts growth, spawning and increase of the metabolic activity in most of the brachiopods, the cold water (polar) brachiopod *Liothyrella uva* (Broderip, 1833) grows much faster in winter than during the summer as an effect of maximizing the efficiency of resource utilization (Peck et al., 1997). Increased metabolic activity due to resource availability and an increase in respiration activity during the cold season could explain the ^{12}C enrichment (i.e. $\delta^{13}C$ negative peaks; McConnaughey, 1988) coupled with maxima of $\delta^{18}O$ values, indicating that these cold-water brachiopods had higher growth rates during the cold seasons. As an alternative explanation, a reduction in primary productivity during the cold seasons could make the seawater lighter (as otherwise ^{12}C would be preferentially taken up in organic matter during photosynthesis), producing minima in $\delta^{13}C$ values in correspondence of maxima in $\delta^{18}O$ values in the shell, explaining the observed pattern. In both cases, a seasonal process involving temperature variation seems to explain well the observed oscillation in $\delta^{18}O$ values, but the negative skewness of $\delta^{18}O$ residual suggests that the former scenario (i.e. increased growth rates during the cold season) is perhaps more suitable to explain the data at this stage (Fig. 10A).

Moreover, at modern similar latitudes, temperature exerts a substantial control on the seasonal change in the dissolution of CO_2 (Gallego et al., 2018), thus affecting the $\delta^{13}C$ values of the brachiopods shell because it reflects the composition of the CO_2 source to a large extent (Ye et al., 2019). Interestingly, in the Wasp Head Formation, the two specimens of *Trigonotreta* show differences in the amplitude of the seasonal signal of both proxies, with the $\delta^{13}C$ values being less variable in the specimen with narrower excursions of the $\delta^{18}O$ values, suggesting that seasonal change in the dissolution of CO_2 could have been a factor also here.

By contrast, taxa from middle and low paleolatitudes do not show any clear oscillation in the isotope ratios, and record $\delta^{18}O$ values skewed to negative values (i.e. positive skewness of the $\delta^{18}O$ residual in Fig. 10A), suggesting that they grew more likely during the warm season. Living taxa have a similar ecological preference for the growing season, with warmer water species spawning year-round, while temperate to colder water species have more clearly defined seasonal periods for breeding (Baird et al., 2013).

The geochemical profile of the athyridid *Araxathtyris* sp. (Ara-Ju) suggests that the isotopic trend is related to growth and aging, as observed in the specimens of *Permophricodothyris* sp. and *Trigonotreta*

sp., once the signal is purged from high frequency signals. Nevertheless, the columnar layer in species of this genus is different from the other analyzed taxa because it develops in the posterior part of the shell and not throughout most of the shell length as in other taxa. However, it shows a record of $\delta^{13}C$ and $\delta^{18}O$ values similar to the complete isotope profiles of *Trigonotreta* sp. and *Permophricodothyris* sp., suggesting that a cross-calibration between taxa is possible once the geochemical signal is purged from the effect of growth rate.

The middle-anterior part of the shell is commonly selected as the most reliable archive to obtain robust values for reconstructing the oxygen isotope composition of seawater (e.g. Brand et al., 2012; Garbelli et al., 2016; Romanin et al., 2018). In this part of the shell, the columnar layer precipitated at a slower growth rate as testified by data from recent taxa (Rollion-Bard et al., 2019). However, often in fossils, the middle-posterior part of the shell is the best-preserved or the only available one for geochemical analyses. So, the finding of a positive correlation between the shell length and the $\delta^{18}O$ record is relevant for the application to the fossil archive, since it underscores the probability of wider paleotemperature range estimates, skewed to lower values, if the posterior part of the shell is used. For example, employing the equation of Brand et al. (2019) and assuming $\delta^{18}O_{sw}$ equal to −1.0 (Frank et al., 2015), the estimate of mean temperature is ~12.9 °C for samples of *Trigonotreta* sp.(Tri-WH-1 and 2) collected at a length > 20 mm. It increases to ~17.8 °C when the samples are collected at a shell length < 20 mm.

4.4. Comparison of $\delta^{18}O$ values in the different localities and implications for the Permian climate

4.4.1. High latitude settings

Based on the specimens from Australia, the calculated mean seasonal difference in seawater surface temperature (ΔSST) is up to 14.6 °C (~8 °C if the range of the anterior portion of the columnar layer is considered, see Table 5 and Fig. 12) at the top of the Wasp Head Formation (late Sakmarian), assuming constant $\delta^{18}O_{sw}$. In the eastern Australia basin, meltwater contribution has been estimated to have varied from 0 to 8.5% during the deposition of the Wasp Head Formation (Frank et al., 2015). Therefore, the ΔSST could have been lower than the estimate above, since the water discharge could produce a significant seasonal change of $\delta^{18}O_{sw}$ in the first 50–100 m of the water depth (Tiwari et al., 2018). The presence of diamictites in the Wasp Head Formation has been interpreted as the results of sea ice and/or released river ice (Tye et al., 1996), but in the upper part of the formation siltstones and sandstones are dominant, indicating limited meltwater discharge.

In the Wandrawandian Siltstone (late Kungurian to Roadian), the ΔSST can be estimated to ~3.7 °C (see Table 5 and Fig. 12) if the $\delta^{18}O_{sw}$ value is assumed as constant. In this setting, based on the finding of glendonite we can constrain the temperatures to the range of its carbonate precursor, the ikaite (Thomas et al., 2007; Beard et al., 2015). This hydrous crystalline calcium carbonate mineral forms from near-freezing up to a theoretical maximum of ~12 °C, when peculiar physicochemical condition of the environment are fulfilled (Purgstaller et al., 2017). On the other hand, brachiopods could not tolerate the specific condition leading to formation of ikaite at the high temperature range (e.g. strong alkaline pH, Mg supersaturation indicating anomalous salinity) and the ikaite decomposed rapidly already around 10–12 °C. Therefore, we use a semi-conservative approach and derive $\delta^{18}O_{sw}$ values for temperatures comprises between 0 and 6 °C employing the eq. (1) reported in Watkins et al. (2014). The calculated $\delta^{18}O_{sw}$ value, at the maximum hypothesized temperature, is about ~ −3.0‰ if the $\delta^{18}O$ minimum values of the overlapping range is used (~0.0‰, Figs. 7B-C, 12). Making the calculation for near-freezing temperatures, the $\delta^{18}O_{sw}$ results ~ −4.0‰ if the $\delta^{18}O$ maximum values of the overlapping range is used (~0.5‰, Figs. 7B-C, 12), a value similar to ~ −4.6‰, estimated by Beard et al. (2015) for the Wandrawandian Siltstone in the Sydney Basin, using bivalves. The calculated seasonal variation of the $\delta^{18}O_{sw}$ is slightly larger than the variability observed in modern high latitudes

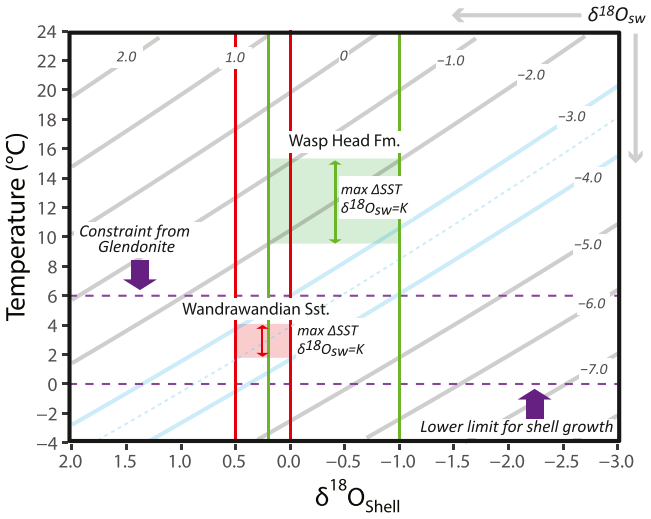

Fig. 12. Estimated of maximum ΔSST for the Wasp Head Formation (green) and Wandrawandian siltstone (red). Lines and shaded areas refer to the estimated for minima and maxima $\delta^{18}O$ values of the overlapping ranges observed from shells of similar ages for the anterior part of the columnar layer. The maximum ΔSST are estimated assuming constant $\delta^{18}O_{sw}$ values equal to −2.0‰ for Wasp Head Formation (Frank et al., 2015) and ~ −3.5‰ for Wandrawandian Siltstone. (For interpretation of the references to color in this figure legend, the reader is referred to the web version of this article.)

Table 5
Estimate of difference in seawater surface temperature (ΔSST) for the different specimens and formations; * (ΔSST) is calculated assuming a constant value of $\delta^{18}O_{sw}$ using the equation of Watkins et al. (2014); bracket values are obtained employing the equation of Brand et al. (2019).

Formation	Specimen	Portion of the columnar layer	Range of $\delta^{18}O$ values		ΔSST*	
			Min	Max		
Wasp Head Formation	Tri-WH-1	Posterior (<25 mm)	−2.5	0.9	16.3 (13.2)	14.6 (11.6)
	Tri-WH-2		−2.5	0.0	12.9 (10.1)	
	Tri-WH-1	Anterior	−1.2	1	10.3 (8.2)	8.0 (6.6)
	Tri-WH-2	(>25 mm)	−1.0	0.2	5.7 (4.5)	
Wandrawandian Siltstone	Tri-Ww	Anterior	0.0	0.6	3.0 (1.9)	3.7 (2.6)
	In-Ww	Anterior	−0.4	0.5	4.5 (3.3)	
Qarari Unit	Car-WKJ	Anterior	−2.1	−1.4	3.8 (3.4)	3.8 (3.4)
	Mar-WKJ	Anterior	−1.9	−1.2	3.7 (3.4)	
Julfa Formation	Per-Ju-1	Anterior	−2.4	−2.2	1.3 (1.0)	1.8 (1.5)
	Per-Ju-2	Overall	−2.6	−2.1	2.9 (2.6)	
	Ara-Ju	Overall	−2.3	−2.1	1.1 (1.0)	
Bulla Member	Com-Bel-2	Posterior	−2.8	−2.5	1.6 (1.7)	
Doubtful Sound	Lio-DS	Middle	0.6	1.2	3.0 (2.5)	

(MacLachlan et al., 2007; Tiwari et al., 2018), also taking into account the water depth where these brachiopods usually live. The presence of ice-rafted dropstones in the Early-Middle Permian Wandrawandian Siltstone (Yang et al., 2018) implies the presence of sea ice and, thus, a contribution of meltwater to explain the amplitude of $\delta^{18}O$ values recorded in the shells. If this is true, also the maximum ΔSST estimated should be further reduced to lower values, approaching a range similar to that observed at modern high latitudes that is ~2 °C (Carton et al., 2015).

In summary, the fluctuations of $\delta^{18}O$ values and variance in the high paleolatitude settings analyzed here (Sydney Basin) were significantly different in the Early vs the Middle Permian (Figs. 8B, 9, Table S2). The amplitude of $\delta^{18}O$ values variation of the specimens from the Wasp Head Formation (late Sakmarian) is more than double that of the shells of the Wandrawandian Siltstone (late Kungurian to Roadian) in a comparable part of the shell (corresponding to a ΔSST of maximum ~8.0 °C Vs ~3.7 °C in the anterior part of the columnar layer), taking into account both the range of overlaps (Table 5). Hence, the results from the Sydney Basin suggest a higher seasonal ΔSST during the deposition of the Wasp Head Formation in the interglacial P1-P2 than for the Wandrawandian Siltstone during P3. This agrees well with the proposition that a reduction of the ice cover could lead to an increase in the ocean seasonal cycle of SST at high latitudes (Carton et al., 2015).

4.4.2. *Middle-low latitude settings*

At about 30° of paleolatitudes, the specimens from Oman show a range of $\delta^{18}O$ values between −2.1 and − 1.2‰. In the late Kungurian, the Qarari Unit was deposited in settings around the storm wave base (Immenhauser et al., 1998; Viaretti et al., 2022). The temperature variation results in a range of ~3.8 °C, assuming a constant composition of $\delta^{18}O_{sw}$. This value is lower than the ΔSST recorded at similar latitudes in modern oceans at shallow depth down to 20 m (e.g. Alexander et al., 2018; Sutton and Bowen, 2019), but the seasonal amplitude of the thermocline in temperate water changes much more with depth than in low or high latitude. The ΔSST recorded could progressively decrease with increasing water depth at the paleolatitudes of the deposition of the Qarari succession. In similar environments, as for the waters of the Arabian Sea in the Persian Gulf, the ΔSST vary from ~9 °C to ~11 °C in the first 10 m, with a progressive drop to ~4 °C at depths of 25 m (Guinehut et al., 2012), and the Qarari brachiopods were living at depths around the storm wave base, which may be around 50 m in a sheltered shelf (Peter and Loss, 2012). Also, increasing evaporation during the summer could increase $\delta^{18}O_{sw}$, resulting in an even smaller range of $\delta^{18}O$ variation of the calcite. This is a reliable alternative to explain the narrow range of $\delta^{18}O$ values of these specimens, considering that the depositional setting of the Qarari Unit (late Kungurian) was an isolated, relatively shallow basin (Viaretti et al., 2022), and thus probably subjected to evaporation.

4.4.3. *Low latitude settings*

The extent of $\delta^{18}O$ values variation in the three specimens from the Julfa Formation (early Wuchiapingian) is relatively narrow, resulting in a mean temperature change within 1.8 °C. The sedimentary succession is deposited at low paleolatitude in the Paleotethys during the early Wuchiapingian in open marine, middle-shelf environments (Gliwa et al., 2020), around the storm wave base. Therefore, the temperature is expected not to vary greatly between summer and winter. At similar latitudes, a relatively constant range of seasonal ΔSST is observed, independent of the water depth (Guinehut et al., 2012). Similarly, in the Bellerophon Formation (late Changhsingian) deposited near the paleoequator in a very shallow marine environment a few meters deep, the $\delta^{18}O$ values range in a narrow interval, resulting in feeble seasonal variations of temperature within an excursion of 1.6 °C. The relatively low ΔSST during the Late Permian agrees well with the paleoclimatic models for this interval of time (Kiehl and Shields, 2005).

5. Conclusion

We have shown that the columnar layer of spiriferid and athyridid brachiopods can be a reliable archive of short-term climate change in the geological record, since it preserves a comparable seasonal variation of $\delta^{18}O$ and $\delta^{13}C$ values across individuals of the same species and across different species and higher taxa.

However, the interpretation of this archive requires caution as the range of $\delta^{18}O$ values in the columnar layer is probably controlled by changes in growth rates during the ontogeny. So, the region of the shell where the proxies are measured must be carefully selected and always specified. Short-term seasonal variations, reconstructed from $\delta^{18}O$ values, were different during the Permian at different paleolatitudes and in different time intervals, but agree well with independently obtained paleoclimatic models. Coupling the isotope ratios time series of the columnar layer with other environmental proxy, such as those constraining salinity and/or bathymetry, has the potential to reconstruct the thermal conditions of past oceans with high precision, even to the scale of seasonality.

Declaration of Competing Interest

The authors declare that they have no known competing financial interests or personal relationships that could have appeared to influence the work reported in this paper.

Data availability

The data are attached as .xlsx file

Acknowledgements

This manuscript has benefited from the valuable comments and suggestions of two anonymous reviewers. The authors also thank prof. Howard Falcon-Lang for his editorial service and advice that helped to improve the manuscript.

This research has benefited from analytical support provided by the technicians and laboratories of the Nanjing Institute of Geology and Palaeontology and Center for Excellence in Life and Paleoenvironment, and the Godwin Laboratory for Palaeoclimate Research at the University of Cambridge.

This study is supported by the Strategic Priority Research Program (B) of the Chinese Academy of Sciences (XDB26000000) and CAS (QYZDY-SSW-DQC023) for SZS, and CG, funding from the China Postdoctoral Science Foundation (Grant N 2016 M591939) and the PIFI initiative of CAS (2018PC0042) to CG. This research is also part of the MCSA project STAMINA - Seasonal Temperatures and Acidification of sensitive Marine settings: Insight of an uNmatched macro-invertebrate Archive (CG). It is a contribution to the project “Biota resilience to global change: biomineralization of planktic and benthic calcifiers in the past, present and future” supported by MURST (PRIN 2017RX9XXXY; LA and RP) and the MIUR-Dipartimenti di Eccellenza 2018-2022 Project (RP and CG).

Appendix A. Supplementary data

Supplementary data to this article can be found online at https://doi.org/10.1016/j.palaeo.2022.111264.

References

Al-Aasm, I., Veizer, J., 1982. Chemical stabilization of low-Mg calcite: an example of brachiopods. J. Sediment. Petrol. 52, 1101–1109.

Alexander, M.A., Scott, J.D., Friedland, K.D., Mills, K.E., Nyel, J.A., Pershing, A.J., Thomas, A.C., 2018. Projected sea surface temperatures over the 21st century: changes in the mean, variability and extremes for large marine ecosystem regions of Northern Oceans. Elem. Sci. Anth. 6, 9. https://doi.org/10.1525/elementa.191.

Angiolini, L., 1993. Ultrastructure of some Permian and Triassic Spiriferida and Arthyridida (Brachiopoda). Riv. It. Paleontol. Strat. 9, 283–306. https://riviste.unimi.it/index.php/RIPS/article/view/8899.

Angiolini, L., Darbyshire, D.P.F., Stephenson, M.H., Leng, M.J., Brewer, T.S., Berra, F., Jadoul, F., 2008. Lower Permian brachiopods from Oman: their potential as climatic proxies. Earth Env. Sci. T. R. So. 98, 327–344. https://doi.org/10.1017/S1755691008075634.

Angiolini, L., Stephenson, M.H., Leng, M.J., Jadoul, F., Millward, D., Aldridge, A., Andrews, J.E., Chenery, S., Williams, G., 2012. Heterogeneity, cyclicity and diagenesis in a Mississippian brachiopod shell of palaeoequatorial Britain. Terra Nova 24, 16–26.

Angiolini, L., Zanchi, A., Zanchetta, S., Nicora, A., Vuolo, I., Berra, F., Henderson, C.M., Malaspina, N., Rettori, R., Vachard, D., Vezzoli, G., 2015. From rift to drift in South Pamir (Tajikistan): Permian evolution of a Cimmerian terrane. J. Asian Earth Sci. 102, 146–169.

Angiolini, L., Crippa, G., Azmy, K., Capitani, G., Confalonieri, G., Della Porta, G., Griesshaber, E., Harper, D.A.T., Leng, M.J., Nolan, L., Orlandi, M., Posenato, R., Schmahl, W.W., Banks, V.J., Stephenson, M.H., 2019. The giants of the phylum Brachiopoda: a matter of diet? Palaeontology 62, 889–917.

Auclair, A.C., Joachimski, M.M., Lécuyer, C., 2003. Deciphering kinetic, metabolic and environmental controls on stable isotope fractionations between seawater and the shell of Terebratalia transversa (Brachiopoda). Chem. Geol. 202, 59–78. https://doi.org/10.1016/S0009-2541(03)00233-X.

Baird, M.J., Lee, D.E., Lamare, M.D., 2013. Reproduction and growth of the terebratulid Brachiopod *Liothyrella neozelanica* Thomson, 1918 from Doubtful Sound, New Zealand. Biol. Bull. 225, 125–136.

Banner, J.L., 1995. Application of the trace element and isotope geochemistry of strontium to studies of carbonate diagenesis. Sedimentology 42, 805–824.

Beard, J.A., Ivany, L.C., Runnegar, B., 2015. Gradients in seasonality and seawater oxygen isotopic composition along the early Permian Gondwanan coast, SE Australia. Earth Planet. Sci. Lett. 425, 219–231.

Brand, U., 2004. Carbon, oxygen and strontium isotopes in Paleozoic carbonate components: an evaluation of original seawater-chemistry proxies. Chem. Geol. 204, 23–44.

Brand, U., Veizer, J., 1980. Chemical diagenesis of a multicomponent carbonate system-1: trace elements. J. Sediment. Petrol. 50, 1219–1236.

Brand, U., Logan, A., Bitner, M.A., Griesshaber, E., Azmy, K., Buhl, D., 2011. What is the ideal proxy of Paleozoic seawater chemistry? Mem. Assoc. Australas. Palaeontol. 41, 9–24.

Brand, U., Logan, A., Hiller, N., Richardson, J., 2003. Geochemistry of modern brachiopods: applications and implications for oceanography and paleoceanography. Chem. Geol. 198, 305–334. https://doi.org/10.1016/S0009-2541(03)00032-9.

Brand, U., Posenato, R., Came, R., Affek, H., Angiolini, L., Azmy, K., Farabegoli, E., 2012. The end-Permian mass extinction: a rapid volcanic CO_2 and CH_4-climatic catastrophe. Chem. Geol. 322–323, 121–144.

Brand, U., Azmy, K., Bitner, M.A., Logan, A., Zuschin, M., Came, R., Ruggiero, E., 2013. Oxygen isotopes and $MgCO_3$ in brachiopod calcite and a new paleotemperature equation. Chem. Geol. 359, 23–31. https://doi.org/10.1016/j.chemgeo.2013.09.014.

Brand, U., Bitner, M.A., Logan, A., Azmy, K., Crippa, G., Angiolini, L., Colin, P., Griesshaber, E., Harper, E.M., Taddei Ruggiero, E.H., Äussermann, V., 2019. Brachiopod-based oxygen-isotope thermometer: update and review. Riv. It. Paleont. Strat. 125, 775–787.

Butler, P.G., Schöne, B.R., 2017. New research in the methods and applications of sclerochronology. Palaeogeogr. Palaeocl. 465, 295–299. https://doi.org/10.1016/j.palaeo.2016.11.013.

Butler, S., Bailey, T.R., Lear, C.H., Curry, G.B., Cherns, L., McDonald, I., 2015. The Mg/Ca-temperature relationship in brachiopod shells: Calibrating a potential palaeoseasonality proxy. Chem. Geol. 397, 106–117.

Butts, S.H., Briggs, D.E.G., 2011. Silicification through time. In: Allison, P., Bottjer, D.J. (Eds.), Taphonomy: Process and Bias Through Time. Springer, pp. 411–434. Topics in Geobiology 32.

Carton, J.A., Ding, Y., Arrigo, K.R., 2015. The seasonal cycle of the Arctic Ocean under climate change. Geophys. Res. Lett. 42, 7681–7686. https://doi.org/10.1002/2015GL064514.

Casella, L.A., Griesshaber, E., Simonet Roda, M., Ziegler, A., Mavromatis, V., Henkel, D., Laudien, J., Häussermann, V., Neuser, R.D., Angiolini, L., Dietzel, M., Eisenhauer, A., Immenhauser, A., Brand, U., Schmahl, W.W., 2018. Micro- and nanostructures reflect the degree of diagenetic alteration in modern and fossil brachiopod shell calcite: a multi-analytical screening (CL, Fe-SEM, AFM, EBSD). Palaeogeogr. Palaeocl. 502, 13–30.

Cisterna, G.A., Shi, G.R., 2014. Lower Permian brachiopods from Wasp Head Formation, Sydney Basin, southeastern Australia. J. Paleontol. 88, 531–544.

Cusack, M., Williams, A., 2001. Chemico-structural differentiation of the organocalcitic shells of rhynconellate brachiopods. In: Brunton, C.H.C., Cocks, L.R.M., Long, S.L. (Eds.), Brachiopods, Past and Present. Taylor & Francis, London, pp. 17–27.

Cusack, M., Huerta, A.P., EIMF, 2012. Brachiopods recording seawater temperature - a matter of class or maturation? Chem. Geol. 334, 139–143. https://doi.org/10.1016/j. chemgeo.2012.10.021.

Farabegoli, E., Perri, M.C., 1998. Permian/Triassic boundary and Early Triassic of the Bulla section (Southern Alps, Italy): lithostratigraphy, facies and conodont biostratigraphy. In: Perri, M.C., Spalletta, C. (Eds.), Southern Alps Field Trip Guidebook, ECOS VII: Giornale di Geologia, vol. 60, pp. 293–311. Spec. Issue.

Farabegoli, E., Perri, M.C., Posenato, R., 2007. Environmental and biotic changes across the Permian-Triassic boundary in western Tethys: the Bulla parastratotype, Italy. In: Yin, H., Warrington, G., Xie, S. (Eds.), Environmental and Biotic Changes during the Paleozoic - Mesozoic Transition. Global Planet. Change 55 (1-3, pp. 109–135.

Fielding, C.R., Frank, T.D., Birgenheier, L.P., Rygel, M.C., Jones, A.T., Roberts, J., 2008. Stratigraphic imprint of the late Palaeozoic Ice Age in eastern Australia: a record of alternating glacial and non-glacial climate regime. J. Geol. Soc. Lond. 165, 129–140.

Fortey, R.A., Heward, A.P., 2015. A new, morphologically diverse Permian trilobite fauna from Oman. Acta Palaeontol. Pol. 60, 201–216.

Frank, T.D., Shults, A.I., Fielding, C.R., 2015. Acme and demise of the late Palaeozoic ice age: a view from the southeastern margin of Gondwana. Palaeogeogr. Palaeocl. 418, 176–192. https://doi.org/10.1016/j.palaeo.2014.11.016.

Gallego, M.A., Timmermann, A., Friedrich, T., Zeebe, R.E., 2018. Drivers of future seasonal cycle changes in oceanic pCO_2. Biogeosciences 15 (5315–5327), 2018. https://doi.org/10.5194/bg-15-5315-2018.

Garbelli, C., 2017. Shell microstructures in Lopingian brachiopods: implications for fabric evolution and calcification. Riv. It. Paleontol. Strat. 123, 541–560.

Garbelli, C., Angiolini, L., Jadoul, F., Brand, U., 2012. Micromorphology and differential preservation of Upper Permian brachiopod low-Mg calcite. Chem. Geol. 299, 1–10. https://doi.org/10.1016/j.chemgeo.2011.12.019.

Garbelli, C., Angiolini, L., Brand, U., Jadoul, F., 2014. Brachiopod fabric, classes and biogeochemistry: implications for the reconstruction and interpretation of seawater carbon isotope curves and records. Chem. Geol. 371, 60–67. https://doi.org/10.1016/j.chemgeo.2014.01.022.

Garbelli, C., Angiolini, L., Brand, U., Shen, S.Z., Jadoul, F., Posenato, R., Azmy, K., Cao, C.Q., 2016. Neotethys seawater chemistry and temperature at the dawn of the latest Permian extinction. Gond. Res. 35, 272–285. https://doi.org/10.1016/j.gr.2015.05.012.

Garbelli, C., Lamare, M.D., Harper, E.M., 2022. Benefits and drawbacks of employing the carbonate shell of brachiopods as an archive of $\delta^{18}O$ seasonality: facts and clues from the living *Calloria inconspicua* (Sowerby, 1846), EGU General Assembly 2022, Vienna, Austria, 23-27 May 2022, EGU22-13210. doi:10.5194/egusphere-egu22-13210.

Garbelli, C., Shen, S.Z., Immenhauser, A., Brand, U., Buhl, D., Wang, W.Q., Zhang, H., Shi, G.R., 2019. Timing of early and Middle Permian deglaciation of the southern hemisphere: Brachiopod-based $^{87}Sr/^{86}Sr$ calibration. Earth Planet. Sci. Lett. 516, 122–135. https://doi.org/10.1016/j.epsl.2019.03.039.

Garbelli, C., Cipriani, A., Brand, U., Lugli, F., Posenato, R., 2022a. Strontium isotope stratigraphic insights on the end-Permian mass extinction and the Permian-Triassic boundary in the Dolomites (Italy). Chem. Geol. 605, 120946 https://doi.org/10.1016/j.chemgeo.2022.120946.

Ghaderi, A., Garbelli, C., Angiolini, L., Ashouri, A.R., Korn, D., Rettori, R., Gharaie, M.H.H., 2014. Faunal change near the end-Permian extinction: the brachiopods of the Ali Bashi mountains, NW Iran. Riv. It. Paleontol. Strat. 120, 27–59.

Ghanizadeh Tabrizi, N., Ghaderi, A., Korn, D., Ashouri, A.R., 2022. Wuchiapingian and early Changhsingian ammonoid biostratigraphy in northwestern Iran. J. Strat. Sediment. Res. 38, 45–66.

Gibbs, M.T., Bowman, M.J., Dietrich, D.E., 2000. Maintenance of Near-Surface Stratification in Doubtful Sound, a New Zealand Fjord. Estuar. Coast. Shelf S. 51, 683–704.

Gliwa, J., Ghaderi, A., Leda, L., Schobben, M., Tomás, S., Foster, W.J., Forel, M.B., Tabrizi, G.N., Grasby, S.E., Struck, U., Ashouri, A.R., Korn, D., 2020. Aras Valley (northwest Iran): high-resolution stratigraphy of a continuous central Tethyan Permian-Triassic boundary section. Foss. Rec. 23 (1), 33–69.

Goodwin, E., Cornelisen, C.C., 2012. Near-surface water temperatures in Doubtful Sound and response to natural and anthropogenic drivers. New Zeal. J. Mar. Fresh. 46 (3), 411–429.

Guinehut, S., Dhomps, A.L., Larnicol, G., Le Traon, P.Y., 2012. High resolution 3D temperature and salinity fields derived from in situ and satellite observations. Ocean Sci. 8 (5), 845–857.

Harlou, R., Ullmann, C.V., Korte, C., Lauridsen, B.W., Schovsbo, N.H., Surlyk, F., Thibault, N., Stemmerik, L., 2016. Geochemistry of Campanian-Maastrichtian brachiopods from the Rørdal-1 core (Denmark): differential responses to environmental change and diagenesis. Chem. Geol. 442, 35–46. https://doi.org/10.1016/j.chemgeo.2016.08.039.

Henderson, C.M., Mei, S.L., Shen, S.Z, Wardlaw, B.R., 2008. Resolution of the reported Upper Permian conodont occurrences from northwestern Iran. Permophiles 5, 2–8.

Huang, N.E., Shen, Z., Long, S.R., Wu, M.C., Shih, H.H., Zheng, Q., Yen, N.C., Tung, C.C., Liu, H.H., 1998. The empirical mode decomposition and Hilbert spectrum for nonlinear and nonstationary time series analysis. P. Roy. Soc. A - Math. Phy. 454, 903–995, 1998.

Imai, N., Terashima, S., Itoh, S., Ando, A., 1996. 1996 compilation of analytical data on nine GSJ geochemical reference samples, "Sedimentary rock series". Geostand. Newsl. 20, 165–216.

Immenhauser, A., Schreurs, G., Peters, T., Matter, A., Hauser, M., Dumitrica, P., 1998. Stratigraphy, sedimentology and depositional environments of the Permian to uppermost cretaceous Batain Group, eastern-Oman. Eclogae Geol. Helv. 91, 217–235.

Immenhauser, A., Schöne, B.R., Hoffmann, R., Niedermayr, A., 2016. Mollusc and brachiopod skeletal hard parts: intricate archives of their marine environment. Sedimentology 63, 1–59.

Kiehl, J.T., Shields, C.A., 2005. Climate simulation of the latest Permian: implications for mass extinction. Geology 33, 757–760. https://doi.org/10.1130/G21654.1.

Krause, S., Liebetraua, V., Löscherb, C.R., Böhma, F., Gorbc, S., Eisenhauera, A., Treude, T., 2018. Marine ammonification and carbonic anhydrase activity induce rapid calcium carbonate precipitation. Geochim.Cosmochim. Acta 243, 116–131.

Leda, L., Korn, D., Ghaderi, A., Hairapetian, V., Struck, U., Reimold, W., 2014. Lithostratigraphy and carbonate microfacies across the Permian-Triassic boundary

near Julfa (NW Iran) and in the Baghuk Mountains (Central Iran). Facies 60, 295–325.
Leven, E., Heward, A., 2013. Fusulinids from isolated Qarari limestone outcrops (Permian), occurring among Jurassic cretaceous Batain Group (Batain Plain, eastern Oman). Riv. It. Paleontol. Strat. 119, 153–162.
Lowenstam, H., 1961. Mineralogy, O^{18}/O^{16} ratios and strontium and magnesium content of recent and fossil brachiopods and their bearing on the history of the oceans. J. Geol. 69, 241-260.MacLachlan, S.E., Cottier, F.R., Austin, W.E.N. and Howe, J.A., 2007. The salinity: δ18O water relationship in Kongsfjorden, western Spitsbergen. Polar Res. 26 https://doi.org/10.1111/j.1751-8369.2007.00016.x, 160e167.
Mackinnon, D.I., 1974. The shell structure in spiriferide brachiopoda. Bull. Br. Mus. Geol. 5, 189–258.
MacLachlan, S.E., Cottier, F.R., Austin, W.E.N., Howe, J.A., 2007. The salinity: $\delta^{18}O$ water relationship in Kongsfjorden, western Spitsbergen. Polar Research 26, 160–167. https://doi.org/10.3402/polar.v26i2.6219.
McConnaughey, T., 1988. ^{13}C and ^{18}O isotopic disequilibrium in biological carbonates: IPatterns. Geochim. Cosmochim. Ac 53, 151–162. https://doi.org/10.1016/0016-7037(89)90282-2.
Mii, H.S., Grossmann, E.L., 1994. Late Pennsylvanian seasonality reflected in the $\delta^{18}O$ and elemental composition of a brachiopod shell. Geology 22, 661–664. https://doi.org/10.1130/0091-7613(1994)022<0661:LPSRIT>2.3.CO;2.
Mii, H., Shi, G.R., Chen, C.J., Chen, Y.Y., 2012. Permian Gondwanaland paleoenvironment inferred from carbon and oxygen isotope records of brachiopod fossils from Sydney Basin, Southeast Australia. Chem. Geol. 291, 87–103. https://doi.org/10.1016/j.chemgeo.2011.10.002.
Muttoni, G., Gaetani, M., Kent, M., Sciunnach, D., Angiolini, L., Berra, F., Garzanti, E., Mattei, M., Zanchi, A., 2009. Opening of the Neo-Tethys Ocean and the Pangea B to Pangea A transformation during the Permian. GeoArabia 14, 17–48. https://doi.org/10.7916/D8SF2TXF.
Ni, S., Krupinski, N.B.Q., Groeneveld, J., Persson, P., Somogyi, A., Brinkmann, I., Knudsen, K.L., Seidenkrantz, M.S., Filipsson, H.L., 2020. Early diagenesis of foraminiferal calcite under anoxic conditions: a case study from the Landsort deep, Baltic Sea (IODP Site M0063). Chem. Geol. 558, 119871 https://doi.org/10.1016/j.chemgeo.2020.119871.
Peck, L.S., Brockington, S., Brey, T., 1997. Growth and metabolism in the Antarctic brachiopod *Liothyrella uva*. Phil. Trans. R. Soc. Lond. B 352, 851–858.
Peter, E.S., Loss, D.P., 2012. Storm and fair-weather wave base: a relevant distinction? Geology 40, 51–514. https://doi.org/10.1130/G32791.1.
Popp, B.N., Anderson, T.F., Sandberg, P.A., 1986. Brachiopods as indicators of original isotopic compositions in some Paleozoic limestones. Geol. Soc. Am. Bull. 97, 1262–1269.
Posenato, R., 2001. The athyridoids of the transitional beds between Bellerophon and Werfen formations (uppermost Permian, Southern Alps, Italy). Riv. Ital. Paleontol. S. 1071, 197–226.
Posenato, R., 2009. Survival patterns of macrobenthic marine assemblages during the end-Permian mass extinction in the western Tethys (Dolomites, Italy). Palaeogeogr. Palaeocl. 280, 150–167.
Posenato, R., 2010. Marine biotic events in the Lopingian succession and latest Permian extinction in the southern Alps (Italy). Geol. J. 45, 195–215. https://doi.org/10.1002/gj.1212.
Posenato, R., 2019. The end-Permian mass extinction (EPME) and the early Triassic biotic recovery in the western Dolomites (Italy): state of the art. Boll. Soc. Paleont. It. 58, 11–34.
Powell, M., Schone, B.R., Jacob, D.E., 2009. Tropical marine climate during the late Paleozoic ice age using trace element analyses of brachiopods. Palaeogeogr. Palaeocl. 280, 143–149. https://doi.org/10.1016/j.palaeo.2009.06.003.
Purgstaller, B., Dietzel, M., Baldermann, A., Mavromatis, V., 2017. Control of temperature and aqueous Mg^{2+}/Ca^{2+} ratio on the (trans-)formation of ikaite. Geoc. Cosmochim Ac. 217, 128–143.
Roark, A., Grossman, E.L., Lebold, J., 2016. Low seasonality in central equatorial Pangea during a late Carboniferous highstand based on high-resolution isotopic records of brachiopod shells. Geol. Soc. Am. Bull. 128, 597–608.
Rollion-Bard, C., Milner Garcia, S., Burckel, P., Angiolini, L., Jurikova, H., Tomašových, A., Henkel, D., 2019. Assessing the biomineralization processes in the shell layers of modern brachiopods from oxygen isotopic composition and elemental ratios: implications for their use as paleoenvironmental proxies. Chem. Geol. 524, 49–66. https://doi.org/10.1016/j.chemgeo.2019.05.031.
Romanin, M., Crippa, G., Ye, F., Brand, U., Bitner, M.A., Gaspard, D., Häussermann, V., Laudien, J.A., 2018. Sampling strategy for recent and fossil brachiopods: selecting the optimal shell segment for geochemical analyses. Riv. Ital. Paleontol. S. 124, 343–359. https://doi.org/10.13130/2039-4942/10193.
Rygel, M.C., Fielding, C.R., Bann, K.L., Frank, T.D., Birgenheier, L., Tye, S.C., 2008. The lower Permian Wasp Head Formation, Sydney Basin: high-latitude, shallow ma-rine sedimentation following the late Asselian to early Sakmarian glacial event in eastern Australia. Sedimentology 55, 1517–1540. https://doi.org/10.1111/j.1365-3091.2008.00955.x.
Schobben, M., Ullmann, C.V., Leda, L., Korn, D., Struck, U., Reimold, W.U., Ghaderi, A., Algeo, T.J., Korte, C., 2016. Discerning primary versus diagenetic signals in carbonate carbon and oxygen isotope records: an example from the Permian-Triassic boundary of Iran. Chem. Geol. 422, 94–107. https://doi.org/10.1016/j.chemgeo.2015.12.013.
Shen, S.Z., Mei, S.L., 2010. Lopingian (Late Permian) high-resolution conodont biostratigraphy in Iran with comparison to South China zonation. Geol. J. 45, 135–161.
Shi, G.R., Du, Y.S., Gong, Y.M., 2007. Soft sediment deformation structures interpreted as sesimite from the Permian Shoalhaven Group, southern Sydney Basin, south-East Australia. Aust. J. Earth Sci. 54, 861–874.
Shi, G.R., Weldon, E.A., Pierson, R.R., 2010. Permian Stratigraphy, Sedimentology and Palaeontology of the Southern Sydney Basin, south-east Australia – A field excursion guide (2010 version) prepared for the 6th International Brachiopod Congress, 1-5 February 2010, Melbourne, Australia. Association of Australasian Palaeontologists (AAP) Field Guide Series No.1.
Shi, G.R., Nutman, A.P., Lee, S., Jones, B.G., Bann, G., 2022. Reassessing the chronostratigraphy and tempo of climate change in the Lower-Middle Permian of the southern Sydney Basin, Australia: integrating evidence from U-Pb zircon geochronology and biostratigraphy. Lithos 410–411, 1–21. https://doi.org/10.1016/j.lithos.2021.106570.
Schöne, B.R., Surge, D.M., 2012. In: Part N, Revised, Volume 1, Chapter 14: Bivalve sclerochronology and geochemistry. Treatise Online 46, pp. 1–24.
Simonet Roda, M., Griesshaber, E., Ziegler, A., Rupp, U., Yin, X., Häussermann, V., Laudien, J., Brand, U., Eisenhauer, A., Checa, A.G., Schmahl, W.W., 2019. Calcite fibre formation in modern brachiopod shells. Sci. Rep. 9, 598.
Sokal, R.R., Rohlf, F.J., 1994. Biometry: The Principles and Practice of Statistics in Biological Research, 3rd ed. . H. Freeman, New York. 887 pp.
Stephenson, M.H., Angiolini, L., Leng, M.J., Darbyshire, D.P.F., 2012. Geochemistry, and carbon, oxygen and strontium isotope composition of brachiopods from the Khuff Formation of Oman and Saudi Arabia. GeoArabia 17, 61–76.
Steuber, T., Veizer, J., 2002. Phanerozoic record of plate tectonic control of seawater chemistry and carbonate sedimentation. Geology 30, 1123–1126. https://doi.org/10.1130/0091-7613(2002)030<1123:PROPTC >2.0.CO;2.
Sutton, P.J.H., Bowen, M., 2019. Ocean temperature change around New Zealand over the last 36 years. New Zeal. J. Mar. Fres. 53, 305–326.
Takayanagi, H., Asami, R., Abe, O., Miyajima, T., Kitagawa, H., Iryu, Y., 2012. Carbon and oxygen-isotope compositions of a deep-water modern brachiopod *Campagea japonica* collected off Aguni-jima, Central Ryukyu Islands, southwestern Japan. Geochem. J. 46, 77–87. https://doi.org/10.2343/geochemj.1.0153.
Takayanagi, H., Asami, R., Abe, O., Miyajima, T., Kitagawa, H., Sasaki, K., Iryu, Y., 2013. Intraspecific variations in carbon- and oxygen-isotope compositions of a brachiopod *Basiliola lucida* collected off Okinawa-jima, southwestern Japan. Geochim. Cosmochim. Ac. 115, 115–136. https://doi.org/10.1016/j.gca.2013.03.026.
Takayanagi, A.R., Otake, T., Abe, O., Miyajima, T., Kitagawa, H., Iryu, Y., 2015. Quantitative analysis of intraspecific variations in the carbon and oxygen isotope compositions of the modern cool-temperate brachiopod *Terebratulina crossei*. Geochim. Cosmochim. Ac. 170, 301–320. https://doi.org/10.1016/j.gca.2015.08.006.
Tiwari, M., Nagoji, S., Kumsr, V., Tripathi, S., Behera, P., 2018. Oxygen isotope-salinity relation in an Arctic fjord (Kongsfjorden): Implications to hydrographic variability. Geosci. Front. 9, 1937–1943. https://doi.org/10.1016/j.gsf.2017.12.007.
Thomas, S.G., Fielding, C.R., Frank, T.D., 2007. Lithostratigraphy of the Mid-Permian Wandrawandian Siltstone, southern Sydney Basin, New South Wales, Australia: record of glaciation and onset of the Hunter-Bowen Event? Aust. J. Earth Sci. 54, 1057–1071. https://10.1080/08120090701615717.
Tye, S.C., Fielding, C.R., Jones, B.G., 1996. Stratigraphy and sedimentology of the Permian Tataterang and Shoalhaven groups in the southernmost Sydney Basin, New South Wales. Aust. J. Earth Sci. 43, 57–69. https://doi.org/10.1080/08120099608728235.
Viaretti, M., Heward, A.P., Gementi, A., Angiolini, L., 2022. Upper Cisuralian-lower Guadalupian brachiopods from the Qarari Unit, Batain plain, northeast Oman: systematics, palaeoecology and correlation. Riv. It. Paleontol. Strat. 128 (3), 643–694 (In press).
Wang, W.Q., Katchinoff, J.A.R., Garbelli, C., Immenhauser, A., Zheng, Q.F., Zhang, Y.C., Yuan, D.X., Shi, Y.K., Wang, J., Planavsky, N., Shen, S.Z., 2021. Revisiting the Permian seawater Sr^{87}/Sr^{86} record: New perspectives from brachiopod proxy data and stochastic oceanic box models. Earth Sci. Rev. 218, 103679 https://doi.org/10.1016/j.earscirev.2021.103679.
Watkins, J.M., Hunt, D.J., Ryerson, F.J., De Paolo, D.J., 2014. The influence of temperature, pH, and growth rate on the $\delta^{18}O$ composition of inorganically precipitated calcite. Earth Planet. Sci. Lett. 404, 332–343.
Williams, A., 1968. Evolution of the shell structure of articulate brachiopods. Spec. Pap. Paleontol. 2, 1–55.
Yamamoto, K., Asami, R., Iryu, Y., 2010. Within-shell variations in carbon and oxygen isotope compositions of two modern brachiopods from a subtropical shelf environment off Amami-o-shima, southwestern Japan. Geochem. Geophys. Geosyst. 11, Q10009. https://doi.org/10.1029/2010GC003190.
Yamamoto, K., Asami, R., Iryu, Y., 2013. Correlative relationships between carbon- and oxygen-isotope records in two cool-temperate brachiopod species off Otsuchi Bay, northeastern Japan. Paleontol. Res. 16, 12–26. https://doi.org/10.2517/1342-8144-17.1.12.
Yang, B., Shi, G.R., Lee, S., Luo, M., 2018. Co-occurrence patterns of ice-rafted dropstones and brachiopods in the Middle Permian Wandrawandian Siltstone of the southern Sydney Basin (southeastern Australia) and palaeoecological implications. J. Geol. Soc. Lond. 175, 850–864. https://doi.org/10.1144/jgs2018-010.
Ye, F.C., Jurikova, H., Angiolini, L., Brand, U., Crippa, G., Henkel, D., Laudien, J., Hiebenthal, C., Šmajgl, D., 2019. Variation in brachiopod microstructure and isotope geochemistry under low-pH-ocean acidification conditions. Biogeosciences 16 (617–642), 2019. https://doi.org/10.5194/bg-16-617-2019.